Original paper

Petrology of nepheline syenite pegmatites in the Oslo Rift, Norway: Zr and Ti mineral assemblages in miaskitic and agpaitic pegmatites in the Larvik Plutonic Complex

Tom ANDERSEN[1]*, Muriel ERAMBERT[1], Alf Olav LARSEN[2], Rune S. SELBEKK[3]

[1] Department of Geosciences, University of Oslo, PO Box 1047 Blindern, N-0316 Oslo

Norway; e-mail: tom.andersen@geo.uio.no

[2] Statoil ASA, Hydroveien 67, N-3908 Porsgrunn, Norway

[3] Natural History Museum, University of Oslo, Sars gate 1, N-0562 Oslo, Norway

* Corresponding author

Abstract. Agpaitic nepheline syenites have complex, Na-Ca-Zr-Ti minerals as the main hosts for zirconium and titanium, rather than zircon and titanite, which are characteristic for miaskitic rocks. The transition from a miaskitic to an agpaitic crystallization regime in silica-undersaturated magma has traditionally been related to increasing peralkalinity of the magma, but halogen and water contents are also important parameters. The Larvik Plutonic Complex (LPC) in the Permian Oslo Rift, Norway consists of intrusions of hypersolvus monzonite (larvikite), nepheline monzonite (lardalite) and nepheline syenite. Pegmatites ranging in composition from miaskitic syenite with or without nepheline to mildly agpaitic nepheline syenite are the latest products of magmatic differentiation in the complex. The pegmatites can be grouped in (at least) four distinct suites from their magmatic Ti and Zr silicate mineral assemblages. Semiquantitative petrogenetic grids for pegmatites in $log\ a_{Na2SiO5} - log\ a_{H2O} - log\ a_{HF}$ space can be constructed using information on the composition and distribution of minerals in the pegmatites, including the Zr-rich minerals zircon, parakeldyshite, eudialyte, låvenite, wöhlerite, rosenbuschite, hiortdahlite and catapleiite, and the Ti-dominated minerals aenigmatite, zirconolite (polymignite), astrophyllite, lorenzenite, titanite, mosandrite and rinkite. The chemographic analysis indicates that although increasing peralkalinity of the residual magma (given by the activity of the $Na_2Si_2O_5$ or *Nds* component) is an important driving force for the miaskitic to agpaitic transition, water, fluoride (HF) and chloride (HCl) activity controls the actual mineral assemblages forming during crystallization of the residual magmas. The most distinctive mineral in the miaskitic pegmatites is zirconolite. At low fluoride activity, parakeldyshite, lorenzenite and wöhlerite are stable in mildly agpaitic systems. High fluorine (or HF) activity favours minerals such as låvenite, hiortdahlite,

rosenbuschite and rinkite, and elevated water activity mosandrite and catapleiite. Astrophyllite and aenigmatite are stable over large ranges of *Nds* activity, at intermediate and low water activities, respectively.

1. Introduction

In 1890, W.C. Brøgger published a seminal work on syenite and nepheline syenite pegmatites from the Larvik Plutonic Complex (LPC) in the Oslo Rift, Norway (Brøgger 1890). These pegmatites contain a variety of Zr and Ti bearing minerals (Table 1), including zircon, titanite, astrophyllite, zirconolite, catapleiite and members of the eudialyte, wöhlerite, rosenbuschite and rinkite groups (Larsen 2010). The presence of volatile-bearing zirconium and titanium minerals such as eudialyte and rinkite in nepheline syenite was only later recognized as a characteristic feature of *agpaitic rocks* (Ussing 1912; Sørensen 1997). Agpaitic rocks are highly peralkaline nepheline syenites in which complex zirconium and titanium silicate minerals have crystallized instead of, or in addition to zircon. Similar mineralogical features are known from highly alkaline rocks ranging in composition from götzenite-bearing nephelinite (e.g. Nyiragongo, East African Rift: Sahama 1978) to elpidite granite (e.g. Strange Lake, Canada: Salvi, Williams-Jones 1995; Gjerdingen, Norway: Raade, Mladeck 1983). It is generally thought that agpaitic liquidus mineral assemblages are stabilized by elevated alkalinity of a silica-undersaturated magma (e.g. Sørensen 1997), but Brøgger (1890) pointed out that volatile components such as fluorine and chlorine in the magma may also have been important for the stabilization of the characteristic Zr and Ti minerals. The factors that control the transition from zircon-present, *miaskitic* to zircon-absent *agpaitic* crystallization regimes have recently been discussed by Andersen et al. (2010) and Marks et al. (2011).

The syenite and nepheline syenite pegmatites in the LPC include zircon-bearing (i.e. miaskitic) as well as transitional (zircon + Na-Ca-Zr-Ti-silicate) and zircon-free agpaitic members. In these pegmatites, the primary zirconium and titanium minerals formed during the early, magmatic stage of crystallization (Larsen 2010). In a previous study, Andersen et al. (2010) applied chemographic analysis to zirconium silicate mineral assemblages in one group of pegmatites in the LPC, and could confirm the importance of the water, fluorine (HF) and chlorine (HCl) activities for the miaskitic to agpaitic transition in that particular system. However, that study was related only to one of the mineralogically distinct types pegmatites in the complex (Larsen 2010), and did not take the titanium-rich mineral assemblages into account. In order to understand the pluton-wide variation in these parameters, and the factors controlling the miaskitic to agpaitic transition on a larger scale, other types of pegmatites and additional mineral assemblages must be considered. In the present paper, we extend the chemographic analysis of Andersen et al. (2010) to cover the whole petrographical range of pegmatites in the LPC, and we include titanium-rich minerals and zirconium minerals such as zirconolite and parakeldyshite in the analysis.

TABLE 1

General mineral formulas for Zr- and Ti- silicates and other minerals from nepheline syenite pegmatites in the Larvik Plutonic Complex

Eudialyte-group	
Eudialyte	$Na_4(Ca,Ce)_2(Fe^{++},Mn,Y)ZrSi_8O_{22}(OH,Cl)_2$ (?)
Ferrokentbrooksite	$Na_{15}Ca_6(Fe,Mn)_3Zr_3NbSi_{25}O_{73}(O,OH,H_2O)_3(Cl,F,OH)_2$
Zirsilite-(Ce)	$(Na,\square)_{12}(Ce, Na)_3Ca_6Mn_3Zr_3Nb(Si_{25}O_{73})(OH)_3(CO_3)\cdot H_2O$

Wöhlerite group	
Wöhlerite	$NaCa_2(Zr,Nb)Si_2O_7(O,OH,F)_2$
Hiortdahlite	$(Ca,Na,Y)_3(Zr,Ti)Si_2O_7(F,O,OH)_2$
Låvenite	$(Na,Ca)_2(Mn,Fe^{++})(Zr,Ti,Nb)Si_2O_7(O,OH,F)_2$

Rosenbuschite group[1]	
Rosenbuschite	$(Ca,Na)_3(Zr,Ti)Si_2O_8F$
Hainite	$Na_4Ca_8(Ti,Zr,Mn,Fe)_3Si_8O_{28}F_8$
Kochite	$Na_2(Na,Ca)_4Ca_4(Mn,Ca)_2Zr_2Ti_2(Si_2O_7)_4(O,F)_4F_4$
Grenmarite	$(Zr,Mn)_2(Zr,Ti)(Mn,Na)(Na,Ca)_4(Si_2O_7)_2(O,F)_4$

Rinkite group	
Mosandrite[2]	$Ti(\square,Ca,Na)_3Ca_4(Si_2O_7)_2[H_2O,OH,F]_4\cdot{\sim}1H_2O$
Rinkite ("Johnstrupite"[3])	$Ti(Na,Ca)_3(Ca,Ce)_4(Si_2O_7)OF_3$
Catapleiite	$(Na,Ca,\square)_2ZrSi_3O_9\bullet2(H_2O)$
Parakeldyshite	$Na_2ZrSi_2O_7$
Lorenzenite	$Na_2Ti_2Si_2O_9$
Aenigmatite	$Na_2Fe_5TiSi_6O_{20}$
Astrophyllite	$(K,Na)_3(Fe,Mn)_7Ti_2Si_8O_{24}(O,OH)_7$
Zirconolite	$CaZrTi_2O_7$
Tritomite-Ce	$(Ce,La,Ca,Y,Th)_5(Si,B)_3(O,OH,F)_{13}$
Pyrochlore	$(Na,Ca)_2Nb_2O_6(OH,F)$

Formulas after Strunz & Nickel (2001) with supplementary data from the *www.mindat.org* database (http://www.mindat.org/strunz.php)
1 Christiansen et al. (2003). 2: Bellezza et al. (2009a), 3: Brøgger (1890), Bellezza et al. (2009b).

2. Geological setting

The Oslo Rift in south-eastern Norway is part of a system of late Carboniferous to Permian continental rifts in northern Europe (Neumann et al. 2004). Rift-related igneous rocks range in composition from alkaline basalt to granite and nepheline syenite, with a large proportion of intermediate, monzonitic intrusive rocks (larvikite) and compositionally equivalent, latitic lavas known as rhomb porphyry (Neuman et al. 2004

and references therein). The Larvik Plutonic Complex (Fig. 1) is a large, composite intrusion making up the southernmost onshore part of the Oslo Rift (Larsen et al. 2008; Dahlgren 2010). The complex is built up by 10 arc-shaped or circular intrusions of hypersolvus monzonite (larvikite) and nepheline syenite (Fig. 1, Petersen 1978). U-Pb dating of magmatic zircon suggests a relatively short period of emplacement (299-292 Ma, Dahlgren 2010), overlapping in time with the main rifting episode with widespread rhomb porphyry volcanism (Larsen et al. 2008). Trace element distribution patterns and radiogenic isotopic signatures of larvikite and rhomb porphyry point towards an origin from the lithospheric mantle (Neumann et al. 2004 and references therein). The rocks of the Larvik Plutonic Complex range from mildly quartz normative in the early ring intrusions, to strongly nepheline normative in the younger intrusions (Fig. 1, Petersen 1978). In the north and west, the complex is penetrated by slightly younger nepheline syenite intrusions, some of which also carry sodalite (Oftedahl, Petersen 1978; Dahlgren 2010). The range in composition of the LPC is explicable by polybaric fractionation of mildly alkaline, mafic parent magma in deep- to middle-crustal magma chambers, combined with a density filtering mechanism (Neumann 1980).
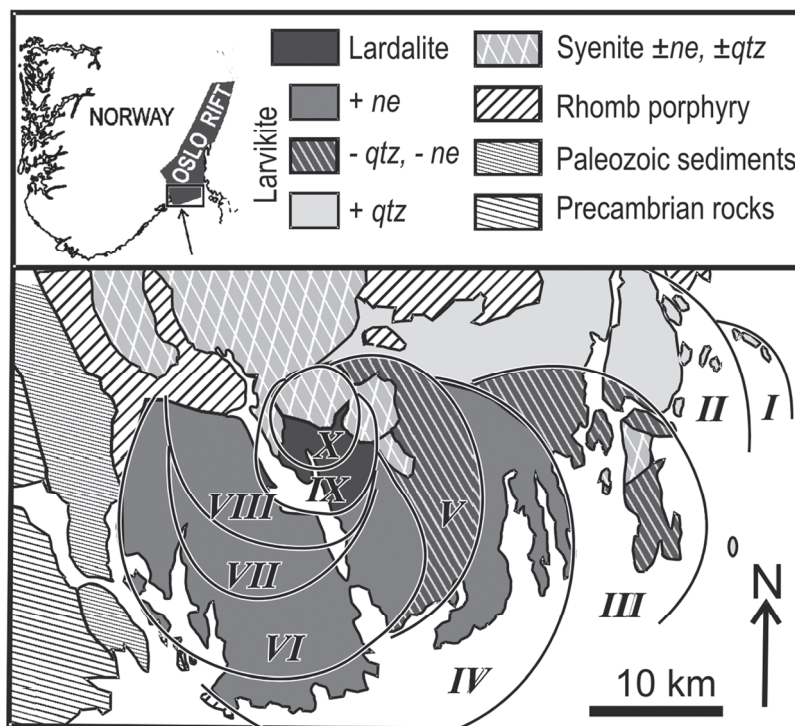

Fig. 1. Simplified geological map of the Larvik Plutonic complex and its surroundings. Based on published maps by Dons and Jorde (1978). Berthelsen et al. (1996), Petersen (1978) and Dahlgren (2010).

Syenite and nepheline syenite pegmatites are relatively common in the Larvik Plutonic Complex; most are hosted by the nepheline-normative ring-segments IV, VI and VII (Fig. 2a). Along the western and south-western margin of the LPC, some pegmatites have intruded contact metamorphosed basalt and rhomb porphyry adjacent to larvikite. The plutonic rocks of the LPC crystallized at shallow-crustal pressures (P ≈ 1 kbar), and reached its solidus at 850-860ºC (Neumann 1976; 1980), which define the maximum pressure and temperature for emplacement of the pegmatites. From the compositions of coexisting Fe-Ti oxides, Neumann (1976) determined a consistent T-f_{O2} cooling trend for the Larvik Plutonic Complex parallel to and less than one $log f_{O2}$ unit below the QFM buffer curve. Oxygen fugacity was buffered during crystallization of the pluton by equilibrium between silicate melt, Fe-Ti oxides and mafic silicate minerals; this probably also applies to the pegmatites in the complex (Andersen et al. 2010).

3. Pegmatites in the LPC and their magmatic Zr and Ti silicate mineral assemblages

Although a relatively complex grouping of the LPC pegmatites based on mineralogy and field observation is possible (e.g. Dahlgren 2010), a simple fourfold division based on characteristic Ti- and Zr silicate mineral assemblages is sufficient for the purpose of this paper. The classification is based on authors' own observations, combined with published data (Andersen et al. 2010; Larsen 2010 and references therein), and information retrieved from the on-line *MinDat.org* database (http://www.mindat.org/index.php). In September 2010, the database contained ca. 2000 separate entries for LPC pegmatites, from ca. 100 localities. Although the database contains information on reported mineral findings rather than coexisting mineral assemblages, and that it is most certainly incomplete, some relevant information may be extracted (Fig. 2).

Syenite pegmatites with or without nepheline, and with zircon as a primary magmatic mineral are abundant in the central and eastern parts of the LPC. These pegmatites are miaskitic rocks, and were assigned to a "Fredriksværn typus" by Brøgger (1890), who also noted the presence of rare "polymignite" (i.e. Fe and Nb bearing zirconolite) in some of them. Zirconolite has since proved to be much more common than assumed by Brøgger and, by September 2010, 20 localities for the mineral in the LPC were listed in the MinDat.org database (Fig. 2b). None of these pegmatites carry eudialyte-group minerals or astrophyllite; the only other Zr-bearing magmatic minerals reported are wöhlerite (Fig. 2b) and zircon. Following Brøgger, the zirconolite-bearing pegmatites are assigned to the *Stavern suite* (from the present-day name of the town known to Brøgger as Fredriksværn). Since zircon also occurs in most of the agpaitic pegmatites (but then in most cases either predating the agpaitic mineral assemblages or formed by alteration of these), the presence of zirconolite may be the most distinctive feature of this group of pegmatites (assemblage M_1 in Table 2).
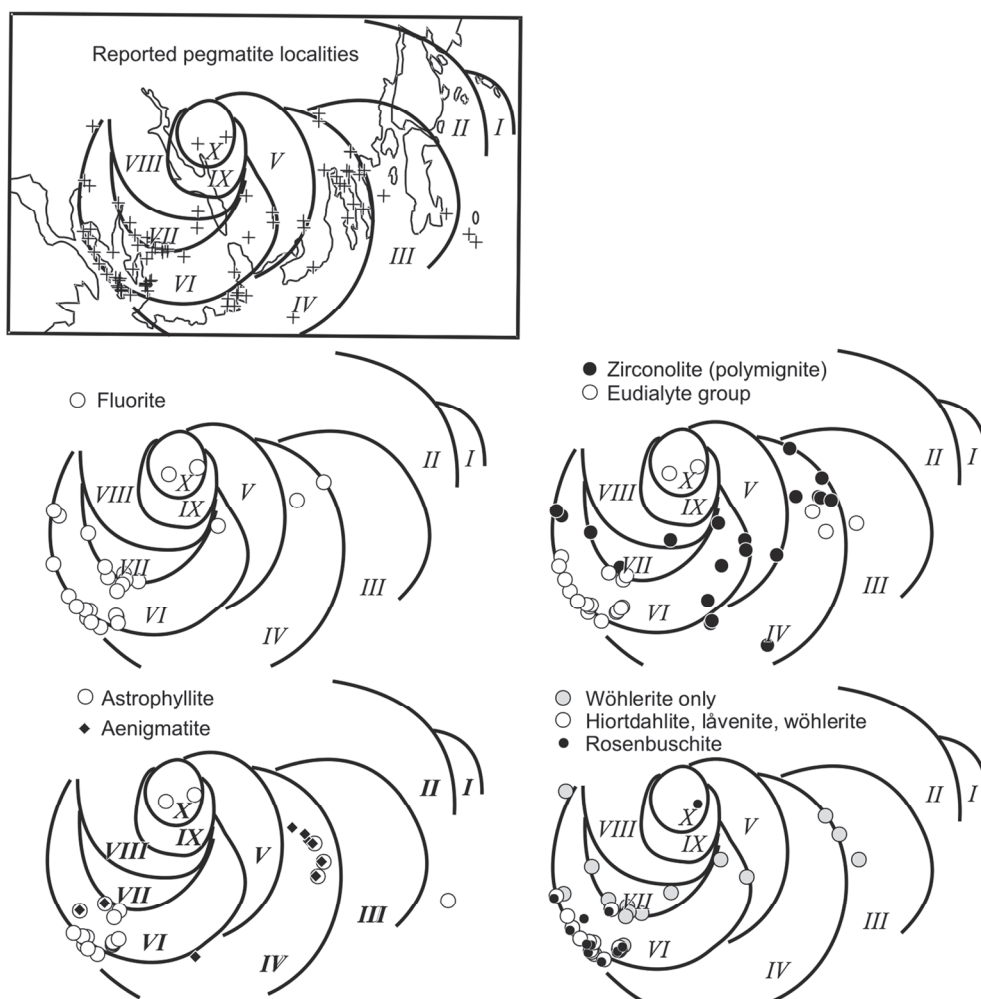
Fig. 2. Distribution maps for indicator minerals in LPC pegmatites, based on data retrieved from the MinDat.org database (http://www.mindat.org/index.php) in September, 2010.
a: All reported pegmatite localities. L: Låven, S: Sagåsen, B: Bratthagen.
b: Reported findings of fluorite and important Zr and Ti minerals in the LPC pegmatites.

Mildly agpaitic nepheline syenite pegmatites characterized by the presence of eudialyte together with minerals of the rosenbuschite, rinkite and wöhlerite groups, including hiortdahlite and låvenite (Fig. 2b) are abundant in the western part of the LPC in the Langesundsfjord archipelago and the adjoining areas on the mainland. Following common usage, these pegmatites are assigned to the *Langesundsfjord suite*. They are mainly contained in larvikite of ring segment VI, but some intrude the country rock of the pluton (Dahlgren 2010). These pegmatites show a variety of Zr silicate mineral assemblages reflecting different, local trends in alkalinity and volatile activities during crystallization of pegmatite magmas (Andersen et al. 2010). Fluorite is abundant in these pegmatites, both as a member of the magmatic mineral assemblage and in late crosscutting veins (Fig. 2b).

A common feature is a change with time from fluorite-free assemblages with wöhlerite together with hiortdahlite or eudialyte (assemblage A in Table 2) to assemblages with fluorite, hiortdahlite, rosenbuschite and eudialyte (assemblage C). Other, locally important assemblages in these pegmatites are zircon + hiortdahlite + fluorite (assemblage D) and hiortdahlite + catapleiite + fluorite (assemblage E), reflecting local trends in water- and alkali activity.

TABLE 2

Some critical Zr and Ti mineral assemblages in LPC pegmatites

---

a: Stavern suite[1]
M_1:   Zircon ± zirconolite ± titanite
M_2:   Zircon + wöhlerite

---

b: Langesundsfjord suite
General[2]:

A: Wöhlerite ± hiortdahlite ± eudialyte
C: Hiortdahlite + rosenbuschite + eudialyte + fluorite ± astrophyllite ± rinkite/hainite
D: Zircon + hiortdahlite + fluorite
E: Hiordahlite + catapleiite + fluorite

Låven pegmatite[2,3] (samples LV01, LV03, LV08, LV09, LV13):
L_A: Mosandrite ± catapleiite ± hainite ± eudialyte ± astrophyllite
L_B: Låvenite + fluorite ± astrophyllite

Sagåsen pegmatite[3] (samples E1, E2, E3, A4, A5):
S_1:   Eudialyte + astrophyllite + wöhlerite
S_2:   Fluorite + zircon + hiortdahlite + astrophyllite (recrystallized)

Sagåsen, boundary zone nepheline syenite[3] (sample SAG1):
SC_1: Zircon + wöhlerite + pyrochlore
SC_2: Rosenbuschite + hainite (?) + fluorite

---

c: Bratthagen suite[4]
B_1:   Zircon + lorenzenite
         Parakeldyshite ± zircon ± catapleiite
B_2:   Rosenbuschite ± fluorite ± astrophyllite ± eudialyte

---

d: Sandefjord suite[5]
F_1:   Aenigmatite
F_2:   Zircon, eudialyte, catapleiite, astrophyllite (the detailed coexistence relationships among these minerals are unconstrained).

References:
[1] Brøgger (1890), Larsen (2010), [2] Andersen et al. (2010), [3] This work, [4] Larsen et al. (1992), Raade and Mladeck (1977), Sæbø (1966), [5] Larsen (2010).

In the present study, samples from the Sagåsen and Låven pegmatites (Fig. 2a) have been studied in some detail, both have complex mineralogy and a multi-stage history of formation (Larsen 2010). The *Sagåsen pegmatite* is a large sill exposed in one of the larvikite quarries in ring segment VI. The major, primary rock-forming minerals are microcline, nepheline, biotite, amphibole, aegirine and sodalite. More than 70 different minerals have been found at this locality. The pegmatite has an early mineral assemblage with eudialyte, coarse-grained astrophyllite, pyrochlore and wöhlerite (assemblage S1 in Table 2). Fluorite forms crosscutting veins along which eudialyte is replaced by zircon, wöhlerite by hiortdahlite and astrophyllite is recrystallized (S2). The pegmatite is surrounded by a thin boundary zone of foliated nepheline syenite, in which zircon and wöhlerite are the primary Zr minerals (assemblage SC_1), zircon has a thin overgrowth of rosenbuschite, and a rosenbuschite-like mineral occurs as interstitial crystals (assemblage SC_2).

The Låven pegmatite has a very complex and heterogeneously distributed mineralogy, and despite of good exposure and nearly two centuries of mineralogical study, neither an unambiguous sequence of coexisting mineral assemblages nor a map of the distribution of minerals in the pegmatite has been established (Brøgger 1890; Liestøl 1956; Larsen 2010). Andersen et al. (2010) pointed out that at least two distinct types of zirconium silicate assemblages can be recognized in this pegmatite, one of which has catapleiite as a characteristic mineral (L_A), suggesting high water activity, whereas the other with låvenite + fluorite (L_B) indicates much lower water activity. The titanium-dominated minerals mosandrite and hainite may be associated with catapleiite in the L_A assemblage in Table 2, whereas astrophyllite occurs in close association with both of these assemblages.

Pegmatites with parakeldyshite, lorenzenite, catapleiite, astrophyllite and eudialyte occur in a small area of ring segment X, where they are associated with a crosscutting, sodalite-bearing foyaite intrusion rather than with rocks belonging to the LPC sensu stricto (Sæbø 1966; Dahlgren 2010). From the locality, these pegmatites are assigned to the *Bratthagen suite*. Coexisting mineral assemblages were described in some detail by Sæbø (1966); Raade and Mladeck (1977) and Larsen et al. (1992). These pegmatites have early, magmatic mineral assemblages with zircon, lorenzenite, parakeldyshite and catapleiite (B_1 assemblages in Table 2). Astrophyllite and rosenbuschite also occur in the pegmatites, but not in grain contact with the B_1 minerals. Fluorite is reported from these pegmatites (Larsen 2010); re-examination of the material studied by Raade and Mladeck (1977) shows that fluorite does not occur in contact with the B_1 minerals. Fluorite, astrophyllite, eudialyte and rosenbuschite are therefore assigned to a later B_2 assemblage.

A group of pegmatites that appear to be transitional between the Stavern and Langesundsfjord suites in terms of mineralogy occur in the eastern part of ring segment IV. These pegmatites contain zircon, aenigmatite, eudialyte, astrophyllite and catapleiite in different combinations. This is a diverse class of intrusions, which are tentatively grouped in the *Sandefjord suite*. Coexisting mineral assemblages in these pegmatites have not been studied in similar detail as the Langesundsfjord and Bratthagen suites, and the list of possible critical assemblages in Table 2 is tentative. Early crystallized aenigmatite has been reported from some localities (Fig. 2b, assemblage F_1 in Table 2). It also appears justified to assign astrophyllite, eudialyte and catapleiite to one or more assemblages representing a main magmatic stage of evolution (assemblage F_2). Fluorite, wöhlerite, hiortdahlite,

rosenbuschite, låvenite or mosandrite are not reported from these localities in the MinDat.org database (Fig. 2b). One single pegmatite in the area has both aenigmatite and zirconolite.

4. Mineral chemistry

4.1. Analytical methods

Scanning electron microscopy and electron microprobe analysis was done at the Department of Geosciences, University of Oslo, and X-ray diffraction studies at the Natural History Museum, University of Oslo. Mineral fragments for XRD and electron microprobe work were separated from the pegmatite matrix under a binocular microscope, samples for EMP analysis were mounted in epoxy and polished. The samples were imaged by backscattered electrons using a Cameca SX100 electron microprobe and a JEOL JSM 6460LV scanning electron microscope with an Oxford Instruments LINK INCA energy dispersive analyser prior to and during the analytical sessions, the BSE images acting as guides for the selection of points to be analysed.

Electron microprobe analysis was performed on a Cameca SX100 fitted with 5 wavelength-dispersive (WDS) spectrometers. An accelerating voltage of 15 kV, beam current of 15 nA and a focused beam were generally used. Beam-sensitive minerals – catapleiite, mosandrite and eudialyte - were analyzed at 10 nA and a beam diameter of 10 μm. Counting time was 10 s on peak (and 5 s on each background positions). Na, F, Cl and K were analyzed first. Prior to analysis, full-range WDS spectra were acquired on several grains of each mineral species in order to identify all elements present and possible interferences between x-ray lines. Background positions for each mineral type were then selected on detailed WDS scans acquired around the x-ray lines of interest.

Calibration standards and x-ray lines used were wollastonite (Si $K\alpha$, Ca $K\alpha$), Al_2O_3 (Al $K\alpha$), pyrophanite (Ti $K\alpha$, Mn $K\alpha$), Fe metal (Fe $K\alpha$), MgO (Mg $K\alpha$) orthoclase (K $K\alpha$), albite (Na $K\alpha$), fluorite (F $K\alpha$), synthetic alforsite (Cl $K\alpha$), Monastery Mine zircon (Zr $L\alpha$), Hf metal (Hf $M\alpha$), Si-Al-Ca glass with 15% ThO_2 (Th $M\alpha$), Nb_2O_5 (Nb $L\alpha$), Ta_2O_5 (Ta $M\alpha$), scheelite (W $M\alpha$), synthetic orthophosphates (Jarosewich, Boatner 1991) for REE and Y (La $L\alpha$, Ce $L\alpha$, Nd $L\beta$, Y $L\alpha$). Matrix corrections were done according to the PAP procedure (Pouchou, Pichoir 1984).

4.2. Astrophyllite

The minerals of the astrophyllite group (general formula, see Table 1) comprise i.a. astrophyllite (*sensu stricto*), kupletskite, niobophyllite and zircophyllite (Piilonen et al. 2003). Astrophyllite from Langesundsfjord and Bratthagen pegmatites have previously been analysed by Piilonen et al. (2003). Here, we present new electron microprobe data from three samples from the Sagåsen pegmatite (Table 3a, Appendix A). Sample A4 consists of primary magmatic astrophyllite intergrown with aegirine, A5 is a fragment of a decimetre-sized crystal of primary magmatic astrophyllite crosscut by BSE-darker veins, and sample E2 consists of fine-grained astrophyllite coexisting with eudialyte, probably

formed or recrystallized during late magmatic or hydrothermal alteration of the primary magmatic mineral assemblage.

TABLE 3a

Electron microprobe analyses of minerals from LPC pegmatites

a: Selected analyses of astrophyllite								
	A5-1	A5-7	A5-11 Vein	A5-13	A5-14	A5-15	A4-20	A4-21	E2-37
Weight percent oxides								
SiO_2	33.45	33.99	35.90	33.88	33.46	34.38	34.24	35.35	33.69
Al_2O_3	1.12	1.23	0.51	1.12	1.16	0.90	1.02	0.66	1.39
Nb_2O_5	0.66	1.59	0.32	0.69	3.15	0.87	1.44	0.22	2.80
ZrO_2	4.25	1.02	0.11	3.98	0.88	0.91	3.25	1.39	4.52
HfO_2	0.12	0.10	0.05	0.27	0.10	0.06	0.12	0.02	0.26
TiO_2	8.74	10.20	11.10	9.03	7.50	11.09	9.04	11.03	7.53
La_2O_3	0.21	0.00	0.02	0.13	0.08	0.12	0.08	0.00	0.00
Ce_2O_3	0.13	0.00	0.01	0.23	0.00	0.15	0.20	0.00	0.00
Nd_2O_3	0.23	0.00	0.00	0.11	0.08	0.03	0.06	0.00	0.06
FeO	22.72	25.58	28.26	23.42	24.08	23.98	17.91	19.84	20.11
MgO	0.94	0.53	0.27	0.64	0.61	0.73	1.04	0.96	0.85
MnO	11.12	9.85	8.45	11.46	11.20	11.41	16.35	16.02	15.61
CaO	0.91	0.89	0.36	0.76	0.72	1.08	0.97	0.83	1.22
Na_2O	2.21	2.32	4.92	2.40	2.39	2.42	2.23	2.70	1.99
K_2O	5.43	5.68	1.42	5.42	5.49	5.39	5.83	5.64	6.14
F	1.30	1.05	1.26	1.05	0.95	1.17	1.40	1.55	1.16
O=-F	-0.55	-0.44	-0.53	-0.44	-0.40	-0.49	-0.59	-0.65	-0.49
Sum	93.02	93.60	92.42	94.15	91.43	94.18	94.59	95.54	96.84

Structural formulas based on 20.00 cations								
Si	7.78	7.76	8.16	7.78	7.84	7.79	7.80	7.85	7.58
Al	0.31	0.33	0.14	0.30	0.32	0.24	0.27	0.17	0.37
Nb	0.07	0.16	0.03	0.07	0.33	0.09	0.15	0.02	0.29
Zr	0.48	0.11	0.01	0.45	0.10	0.10	0.36	0.15	0.50
Hf	0.01	0.01	0.00	0.02	0.01	0.00	0.01	0.00	0.02
Ti	1.53	1.75	1.90	1.56	1.32	1.89	1.55	1.84	1.28
La	0.02	0.00	0.00	0.01	0.01	0.01	0.01	0.00	0.00
Ce	0.01	0.00	0.00	0.02	0.00	0.01	0.02	0.00	0.00
Nd	0.02	0.00	0.00	0.01	0.01	0.00	0.00	0.00	0.00
Fe	4.42	4.89	5.37	4.50	4.72	4.54	3.41	3.68	3.78
Mg	0.33	0.18	0.09	0.22	0.21	0.25	0.35	0.32	0.28
Mn	2.19	1.91	1.63	2.23	2.22	2.19	3.15	3.01	2.98
Ca	0.23	0.22	0.09	0.19	0.18	0.26	0.24	0.20	0.29
Na	0.10	1.03	2.17	1.07	1.08	1.06	0.99	1.16	0.87
K	1.61	1.66	0.41	1.59	1.64	1.56	1.69	1.60	1.76
F	0.96	0.76	0.91	0.77	0.70	0.84	1.01	1.09	0.82

The full set of data is found in Appendix A

Electron microprobe analyses of minerals from LPC pegmatites

b: Eudialyte-group minerals											
	E1-22	E1-23	E1-24	E1-25	E1-26	E1-27	E1-30	E3-31	E3-34	E3-35	E3-36
Weight percent oxides											
SiO_2	45.07	44.05	43.85	43.39	43.72	43.77	43.98	43.88	44.20	44.08	44.19
Al_2O_3	n.d	n.d	n.d	n.d	n.d	n.d	n.d	n.d	n.d	n.d	n.d
Nb_2O_5	3.03	3.24	2.73	3.12	1.48	2.99	3.03	2.98	3.07	3.08	3.12
ZrO_2	11.23	10.65	10.80	10.29	9.62	10.85	10.66	10.77	10.46	10.85	10.41
HfO_2	0.55	0.60	0.45	0.21	2.21	0.43	0.47	0.43	0.60	0.45	0.56
TiO_2	n.d	0.06	0.08	n.d.	n.d	0.07	0.05	n.d.	n.d.	n.d	0.05
ThO_2	n.d.	n.d.	n.d.	n.d.	n.d.	n.d	n.d.	n.d.	n.d.	n.d.	n.d.
La_2O_3	2.44	2.31	2.26	2.75	1.71	2.20	2.29	2.14	2.14	2.41	2.62
Ce_2O_3	3.79	3.93	3.46	3.94	2.80	3.19	3.65	2.79	2.83	2.96	3.24
Nd_2O_3	0.73	0.67	0.51	0.80	0.41	0.67	0.57	0.40	0.49	0.58	0.40
Y_2O_3	1.39	1.28	1.16	1.27	1.96	1.16	1.54	0.81	0.67	0.91	0.54
FeO	3.17	3.11	3.16	1.51	0.79	3.23	2.44	2.99	3.00	3.07	3.21
MnO	6.07	6.37	6.61	9.19	9.52	5.93	7.42	4.86	4.91	5.25	5.21
CaO	7.86	7.87	7.70	6.70	6.45	7.68	7.32	10.32	10.94	9.55	9.79
Na_2O	11.10	11.20	11.55	11.25	11.60	11.27	11.35	10.85	10.90	11.03	11.10
K_2O	0.29	0.31	0.25	0.16	0.21	0.28	0.28	0.36	0.31	0.29	0.31
F	n.d	n.d	n.d	n.d	n.d	n.d	n.d	n.d	n.d	n.d	n.d
Cl	0.75	0.77	0.82	0.88	1.11	0.77	0.78	0.72	0.75	0.92	0.88
O=-Cl	-0.17	-0.17	-0.18	-0.20	-0.25	-0.17	-0.18	-0.16	-0.17	-0.21	-0.20
Sum	97.32	96.24	95.30	95.32	93.37	94.32	95.64	94.13	95.11	95.25	95.42

Structural formulas based on 29.00 cations and ion-allocations according to Pfaff et al. (2010) and Andersen et al. (2010)												
Si	T	24.00	24.00	24.00	24.00	24.00	24.00	24.00	24.00	24.00	24.00	24.00
Si	M4	1.00	1.00	1.00	1.00	1.00	1.00	1.00	1.00	1.00	1.00	1.00
Si	M3	0.10	0.09	0.16	0.23	0.51	0.09	0.15	0.15	0.20	0.11	0.19
Zr+Hf	M3	0.14	0.05	0.09	0.00	0.10	0.10	0.05	0.08	0.01	0.09	0.00
Nb	M3	0.76	0.84	0.71	0.77	0.39	0.78	0.78	0.77	0.79	0.79	0.80
Ti	M3		0.02	0.03			0.03	0.02			0.01	0.00
Zr+Hf	Z	3.00	3.00	3.00	2.95	3.00	3.00	3.00	3.00	3.00	3.00	2.98
Nb	Z				0.05							
Fe	M2	1.48	1.48	1.52	0.74	0.39	1.55	1.17	1.43	1.43	1.46	1.53
Mn	M2	1.52	1.52	1.48	2.26	2.61	1.45	1.83	1.57	1.57	1.54	1.47
REE	M1	1.31	1.20	1.26	1.82	1.66	1.28	1.51	0.00	0.00	0.17	0.02
Ca	M1	3.35	3.25	3.01	1.91	2.25	3.29	2.73	5.21	5.20	4.83	4.93
Mn	M1	1.34	1.55	1.73	2.26	2.09	1.43	1.76	0.79	0.80	1.00	1.05
Ca	N	1.34	1.55	1.73	2.26	1.78	1.43	1.76	1.12	1.48	1.00	1.05
REE	N	0.52	0.63	0.40	0.16	0.00	0.35	0.32	1.37	1.35	1.35	1.45
Na	N	11.98	12.36	12.85	12.68	13.12	12.53	12.58	12.05	12.05	12.18	12.27
K	N	0.21	0.22	0.18	0.12	0.15	0.20	0.20	0.26	0.23	0.21	0.23
□+H_3O^+	N	1.95	1.23	0.84	0.77	0.94	1.50	1.14	1.19	0.90	1.27	1.00
Cl	X	0.70	0.74	0.79	0.86	1.10	0.75	0.75	0.70	0.72	0.89	0.85
OH	X	1.30	1.26	1.21	1.14	0.90	1.25	1.25	1.30	1.28	1.11	1.15

n.d.: Not detected at detection limits: Al_2O_3: 0.03wt%, TiO_2: 0.04 wt% ,ThO_2: 0.1 wt%, F: 0.4 wt%

□: Vacancy

Electron microprobe analyses of minerals from LPC pegmatites

c: Selected analyses of rinkite- and rosenbuschite group minerals											
	LV01 #01 Koc (?)	LV01 #02 Koc (?)	LV01 #04 Hio	LV01 #2 Mos	LV01 #8 Mos	LV08 #M05 Mos	LV08 #M06 Mos	LV03 #114 Hai	LV03 #115 Hai	LV09 #23 Ros	SAG1 #48 Ros	SAG1 #51 Hai
Weight percent oxides												
SiO_2	30.82	30.82	30.27	29.98	28.82	29.01	29.32	29.79	30.04	30.25	31.37	30.90
ZrO_2	11.31	10.90	16.90	1.41	1.14	1.67	1.76	5.02	3.32	9.95	16.02	6.89
HfO_2	0.27	0.01	0.43	0.10	0.04	0.03	0.04	0.15	0.07	0.22	0.23	0.14
Nb_2O_5	1.07	1.02	2.10	1.52	1.50	1.53	1.85	1.53	1.18	1.07	0.08	0.99
ThO_2	n.d.	n.d.	n.d.	0.79	0.85	0.77	1.03	0.24	0.18	n.d.	n.d.	0.11
TiO_2	9.90	10.45	0.93	9.15	9.44	9.79	9.83	8.14	8.26	7.46	7.90	8.16
Y_2O_3	2.19	2.46	1.00	0.07	4.09	2.91	3.04	3.45	3.84	3.39	0.03	2.00
La_2O_3	0.18	0.10	0.17	3.93	4.58	3.75	3.77	0.90	1.52	0.44		0.72
Ce_2O_3	0.32	0.30	0.45	8.69	8.82	8.22	8.28	2.12	3.33	1.21	0.08	1.76
Nd_2O_3	0.12	0.25	0.16	3.01	3.36	2.41	2.77	0.62	1.12	0.38		0.76
Al_2O_3	n.d.	n.d.	n.d.	0.24	0.42	1.03	0.97	n.d.	n.d.	n.d.	0.05	n.d.
CaO	22.04	22.71	31.48	18.70	16.62	18.03	17.55	30.90	30.13	26.47	28.06	31.93
FeO	0.37	0.28	1.24	0.02	0.04	0.18	0.10	0.36	0.26	0.28	0.47	0.46
MnO	4.31	3.40	1.32	0.23	0.28	0.29	0.45	0.67	0.54	1.74	0.96	0.63
Na_2O	10.02	9.96	7.15	2.11	1.41	1.75	1.43	7.50	7.76	8.62	9.14	7.45
K_2O	0.02	0.00	0.02	0.09	0.11	0.17	0.16	0.01	0.01	0.01	0.01	0.02
F	7.59	7.82	7.86	2.60	2.56	1.94	2.41	7.61	7.66	8.05	7.74	8.75
O=-F	-3.19	-3.29	-3.31	-1.10	-1.08	-0.82	-1.02	-3.21	-3.22	-3.39	-3.26	-3.68
Total	97.37	97.21	98.16	81.53	83.02	82.66	83.76	95.80	95.99	96.21	98.88	98.01
Structural formulas based on 4.000 Si												
Si	4.00	4.00	4.00	4.00	4.00	4.00	4.00	4.00	4.00	4.00	4.00	4.00
Zr+Hf	0.73	0.69	1.11	0.10	0.08	0.11	0.12	0.33	0.22	0.65	1.00	0.44
Ti	0.97	1.02	0.09	0.92	0.99	1.02	1.01	0.82	0.83	0.74	0.76	0.79
Nb	0.06	0.06	0.13	0.09	0.09	0.10	0.11	0.09	0.07	0.06	0.00	0.06
Th				0.02	0.03	0.02	0.03	0.01	0.01			0.00
REE[1]	0.18	0.20	0.11	0.77	1.15	0.94	0.96	0.43	0.56	0.34	0.01	0.29
Al				0.04	0.07	0.17	0.16	0.00			0.01	
Fe	0.04	0.03	0.14	0.00	0.00	0.02	0.01	0.04	0.03	0.03	0.05	0.05
Mn	0.47	0.37	0.15	0.03	0.03	0.03	0.05	0.08	0.06	0.19	0.10	0.07
Ca	3.06	3.16	4.46	2.67	2.47	2.66	2.57	4.44	4.30	3.75	3.83	4.43
Na	2.52	2.51	1.83	0.54	0.38	0.47	0.38	1.95	2.00	2.21	2.26	1.87
K	0.00	0.00	0.00	0.02	0.02	0.03	0.03	0.00	0.00	0.00	0.00	0.00
F	3.11	3.21	3.28	1.10	1.12	0.85	1.04	3.23	3.22	3.37	3.12	3.58
SumCat	12.04	12.04	12.01	9.20	9.31	9.57	9.42	12.20	12.08	11.98	12.03	12.01
Vac				2.80	2.69	2.43	2.58			0.02		

Abbreviations: Mos= Mosandrite, Ros= Rosenbuschite, Koc= Kochite, Hai= Hainite, Hio= Hiortdahlite.
1: REE= La+Ce+Nd+Y
The full set of data is found in Appendix B
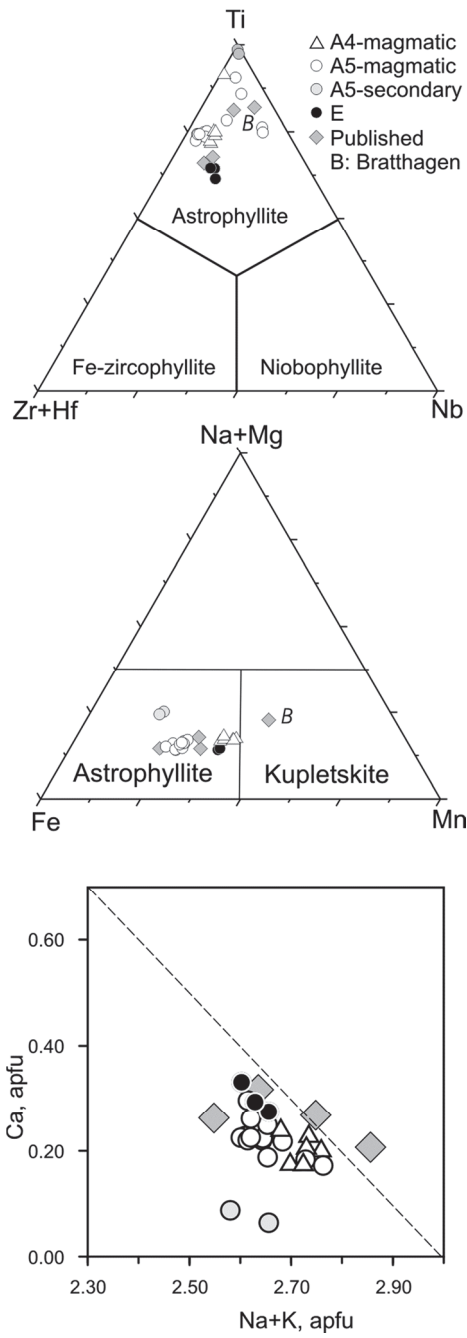
Fig. 3. Compositions of astrophyllite from the Sagåsen pegmatite, data from Table 3a and Appendix A. Grey diamonds are analyses of astrophyllite-group minerals by Piilonen et al. (2003), the point marked B is from Bratthagen.

All of the present analyses fall within the astrophyllite field (Fig. 3), and within the range of published analyses of astrophyllite-group minerals from the LPC (Piilonen et al. 2003). The maximum manganese content is found in the magmatic astrophyllite in sample A4, which plots close to the boundary towards kupletskite. Fluorine varies from 0.7 to 1.0 a.p.f.u., and charge balance requirements suggest that the remainder of this anion site is filled by O^{2-}. Ti/(Ti+Zr+Hf) ranges from ca 0.75 to 1.0, the highest values found in BSE-dark veins in sample A5. These veins have an astrophyllite composition, but lower K and Ca and higher Na than the host crystal. The late magmatic or hydrothermal astrophyllite in sample E2 is lower in Ti and marginally higher in Ca than the magmatic astrophyllite in samples A4 and A5, but overlaps with the others in Fe/Mn ratio (Fig. 3).

4.3. Eudialyte

The general formula of the eudialyte group can be written: *[N(I)N(2)N(3)N(4)N(5)]₃-[M(la)M(lb)]₃M(2)₃M(3)M(4)Z₃[Si₂₄O₇₂]O₄X₂*, in which X = Cl, F, OH or CO_3 and Z = Zr, Ti and N and M are cation sites incorporating Na, K, Ca, Nb, Fe, Mn; Si is also accommodated in an off-ring, tetrahedral position (M(4)), and it competes with Nb and other high-valence ions in 4 to 6 coordinated M(3) position (Johnsen et al, 2003). Some relevant, theoretical endmember compositions are given in Table 1. Eudialyte analyses have been recalculated to structural formulas using the same procedure as in Andersen et al. (2010), which is a slightly modified version of the ion assignment algorithm of Pfaff et al. (2010).

Eudialyte has been analysed in two samples (E1, E3) from the Sagåsen pegmatite, which supplements analyses from Langesundsfjord suite pegmatites published by Andersen et al. (2010), and analyses from Sagåsen itself including minor and trace components by Larsen et al. (2005). Compared to the analyses published by Andersen et al. (2010), the present eudialytes (Table 3b) have clearly higher Mn/(Mn+Fe) ratio, lower $Si_{M(3)}$ and lower combined vacancies and H_3O^+ in the *N*-position (Fig. 4). An appropriate characterization of the mineral in terms of endmembers would be "feklichevite-zirsilite solid solution", with some domains ranging towards kentbrooksite.
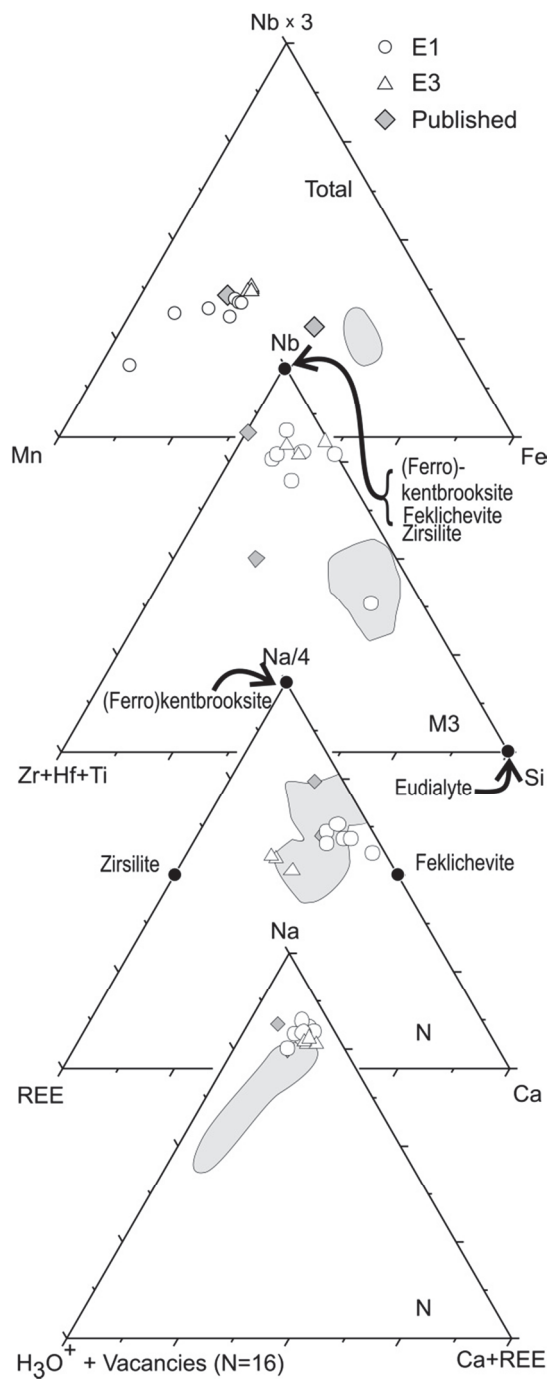
Fig. 4. Composition of eudialyte group minerals in the Sagåsen pegmatite, data from Table 3b. The grey fields are the ranges of eudialyte group minerals in Langesundsfjord suite pegmatites analysed by Andersen et al. (2010), grey rhombs are analyses from the Sågåsen pegmatite by Larsen et al. (2005).

4.4. Mosandrite and rosenbuschite group minerals

The rinkite (monoclinic) and rosenbuschite (triclinic) mineral groups are Ti and / or Zr-rich sorosilicates that can be represented by general formulas of the type $A_{6+x}B_{2-x}(Si_2O_7)_2(X)_4$ in which A= Na, Ca, Fe, Mn, Y, REE, B= Ti, Zr, Nb and X= F, O (and OH, H_2O in mosandrite, Bellezza et al. 2009a). For the compositions of individual species, see Table 1. The structures of the two groups differ mainly in the mode of stacking of polyhedral sheets (Sokolova 2006).

Mosandrite was first described from the Låven pegmatite by Erdmann (1840); after considerable controversy (e.g. Sokolova, Cámara 2008), its status as a hydrous, cation-deficient species belonging to the rinkite group was finally established by Bellezza et al. (2009a). From new chemical and crystallographical data on the original material studied by Brøgger (1890), Bellezza et al. (2009b) could demonstrate that the suspect mineral "johnstrupite" is, in fact, identical with rinkite. Hainite is a Ca and Ti rich member of the rosenbuschite group, and was first reported from a pegmatite in the Langesundsfjord archipelago by Christiansen et al. (2003). Kochite (Christiansen et al. 2003) is a member of the rosenbuschite group with low Ca and intermediate Ti/(Zr+Ti); it has not previously been reported from the Oslo Rift. In this study we report electron microprobe analyses of mosandrite, rosenbuschite, hainite and possible kochite from Låven island (Table 3c, Appendix B), based on material in the mineral collection of the Natural History Museum of the University of Oslo, which was collected by G.B. Liestøl in the 1950s.

Samples LV08 and LV13 give cation-deficient composition with high REE and Ti, low Na/(Na+Ca) and Ti/(Ti+Zr)>>1 (Fig. 5), comparable to published analyses of mosandrite from the LPC (Brøgger 1890; Bellezza et al. 2009a). Sample LV01 consists of fragments of one or more large, brown mosandrite crystal, intergrown with heterogeneous crystal aggregates consisting of a rosenbuschite-like fibrous mineral, zircon and a REE silicate tentatively identified as tritomite-(Ce) from qualitative EDS analysis in the electron microprobe. The main mineral is a cation-deficient mosandrite similar to the one in LV08 and LV013. The fibrous aggregates consist of a rosenbuschite-like mineral whose composition is close to kochite (Fig. 3), and a high-Zr phase with hiortdahlite-like composition.

Fig. 5. Composition of rosenbuschite and rinkite group minerals from the Låven pegmatite, data from Table 3c and Appendix B. Outlines mark the ranges of rosenbuschite and wöhlerite group minerals in Langesundsfjord suite pegmatites reported by Andersen et al. (2010). *Woe*: wöhlerite, *Lav*: Låvenite, *Ros*: rosenbuschite, *Hio*: Hiortdahlite. Stars indicate published analyses of rinkite and rosenbuschite group minerals: 1: Hainite, Christiansen et al. (2003). 2: Kochite, Christiansen et al. (2003). 3: Mosandrite (= rinkite ?) Sokolova and Cámara (2008)

4: Mosandrite, Brøgger (1890). 5: Mosandrite, Bellezza et al. (2009a). 6: "Johnstrupite" (i.e. rinkite), Brøgger (1890). 7: Rinkite, Bellezza et al. (2009b).

1: Hainite, Christiansen et al. (2003)
2: Kochite, Christiansen et al. (2003)
3: Mosandrite (= rinkite ?) Sokolova & Camara (2008)
4: Mosandrite, Brøgger (1890)
5: Mosandrite, Bellezza et al. (2009a)
6: "Johnstrupite" (i.e. rinkite), Brøgger (1890)
7: Rinkite, Bellezza et al. (2009b)

LV09 consists of rosenbuschite, with composition and range of Ti/(Ti+Zr) comparable to that observed in rosenbuschite from other Langesundsfjord suite pegmatites by Andersen et al. (2010). All but one analysis of LV03 cluster around a titanium-rich composition very close the hainite from a LPC pegmatite analysed by Christiansen et al. (2003). The one outlying analysis is a cation-deficient, REE-rich mosandrite (analysis LV03#116).

The overgrowths on zircon in the boundary zone of the Sagåsen pegmatite (sample SAG1) consist of rosenbuschite similar to that in LV09. The interstitial, rosenbuschite-like crystals in the same sample have lower Zr and higher Ti, and are intermediate between rosenbuschite and hainite in composition (Fig. 5).

5. Chemographic analysis

Andersen et al. (2010) constructed a petrogenetic grid for the zirconium silicate minerals of the Langesundsfjord suite pegmatites (i.e. the present assemblages - type A, C, D and E) in the 13-component system $NaO_{0.5} - KO_{0.5} - CaO - FeO - REEO_{1.5} - ZrO_2 - TiO_2 - NbO_{2.5} - AlO_{1.5} - SiO_2 - HO_{0.5} - FO_{-0.5} - ClO_{-0.5}$. Assuming that the magma was saturated with the major rock-forming minerals of the pegmatites (microcline, albite, nepheline, biotite (hydroxy annite), pyroxene (hedenbergite component of aegirine-augite, Murad 2006), and the widespread minor or accessory mineral pyrochlore, and that TiO_2 and REE_2O_3 were externally buffered by phases not considered in the analysis (titanomagnetite, REE silicates and phosphates), it was possible to construct a grid of divariant planes and univariant lines in 3D $log\ a_{Nds} - log\ a_{H2O} - log\ a_{HF}$ space that was consistent with the observed mineral assemblages and which showed the relative effect of volatile activities and excess alkalinity on zirconium silicate mineralogy (Nds: the $Na_2Si_2O_5$ component). The same principles will be applied in the present study. Phase compositions used to balance melt-mineral reactions are given in Table 4.

TABLE 4

Mineral formulas of Ti- and Zr rich silicates and related minerals in the LPC

Hainite, Teineholmen (Christiansen et al., 2003):
$Na_{1.99}Ca_{4.16}(Fe,Mn)_{0.16}REE_{0.35}Nb_{0.04}Ti_{0.80}Zr_{0.25}(\square)_{0.10}Si_4O_{14}F_{3.24}O_{0.76}$
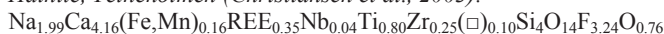
Hainite, LV03, Låven (this work):
$Na_{1.69}Ca_{4.13}(Fe,Mn)_{0.14}REE_{0.45}Nb_{0.07}Ti_{0.79}Zr_{0.25}(\square)_{0.29}Si_4O_{14}F_{2.81}O_{1.19}$
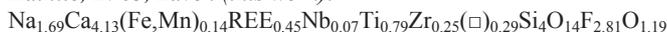
"Johnstrupite", Barkevik area (Brøgger, 1890):
$Na_{1.70}Ca_{3.90}(Fe,Mn)_{0.05}REE_{0.72}Nb_{0.00}Ti_{0.75}Zr_{0.18}(\square)_{0.68}Si_4O_{14}F_{2.48}(O,OH,H_2O)_{1.52}$
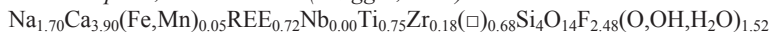
*Rinkite ("Jonstrupite"), Bellezza et al. (2009b); Rin:
$Na_{2.06}C_{4.21}(Fe,Mn)_{0.04}REE_{0.72}Nb_{0.07}Ti_{0.71}Zr_{0.09}(\square)_{0.09}Si_4O_{14}F_{2.81}O_{1.19}$
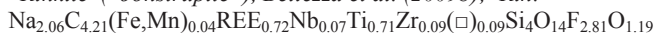
Mosandrite (=rinkite ?), Låven (Sokolova & Camara, 2008):
$Na_{1.98}Ca_{3.89}(Fe,Mn)_{0.00}REE_{0.87}Nb_{0.08}Ti_{0.86}Zr_{0.05}(\square)_{0.26}Si_4O_{14}F_{3.18}(O,OH,H_2O)_{0.82}$

Mosandrite, Brøgger (1890):
$Na_{0.62}Ca_{3.14}(Fe,Mn)_{0.10}REE_{1.03}Nb_{0.00}Ti_{0.52}Zr_{0.47}(\square)_{2.10}Si_4O_{14}F_{0.85}(O,OH,H_2O)_{3.15}$
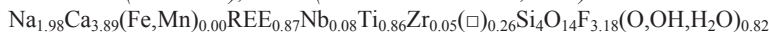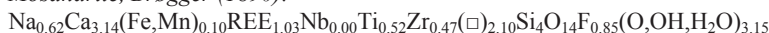
Mosandrite, Låven (Bellezza et al. 2009a); Mos:
$Na_{0.29}Ca_{3.70}(Fe,Mn)_{0.10}REE_{1.06}Nb_{0.09}Ti_{0.93}Zr_{0.10}(\square)_{1.70}Si_4O_{14}F_{0.92}(H_2O)_{3.08}\cdot 0.53H_2O$
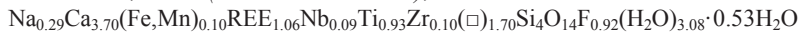
Mosandrite, LV01, Låven (this work):
$Na_{0.19}Ca_{2.52}(Fe,Mn)_{0.11}REE_{0.99}Nb_{0.11}Ti_{1.05}Zr_{0.12}(\square)_{2.88}Si_4O_{14}F_{1.62}(O,OH,H_2O)_{2.38}$
$Na_{0.40}Ca_{2.42}(Fe,Mn)_{0.04}REE_{0.89}Nb_{0.09}Ti_{0.97}Zr_{0.08}(\square)_{3.08}Si_4O_{14}F_{0.85}(O,OH,H_2O)_{3.15}$
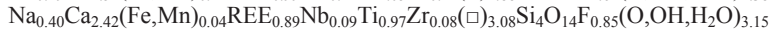
Mosandrite, LV08, Låven (this work):
$Na_{0.32}Ca_{2.18}(Fe,Mn)_{0.05}REE_{1.15}Nb_{0.12}Ti_{1.05}Zr_{0.11}(\square)_{2.98}Si_4O_{14}F_{0.76}(O,OH,H_2O)_{3.24}$
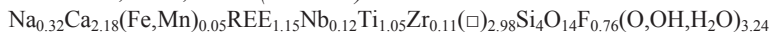
Mosandrite, LV13, Låven (this work):
$Na_{0.15}Ca_{2.32}(Fe,Mn)_{0.54}REE_{1.23}Nb_{0.10}Ti_{1.06}Zr_{0.13}(\square)_{2.43}Si_4O_{14}F_{0.17}(O,OH,H_2O)_{3.83}$
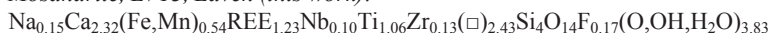
Kochite, Grønland (Christiansen et al., 2003):
$Na_{2.72}Ca_{2.94}(Fe,Mn)_{0.65}REE_{0.06}Nb_{0.10}Ti_{0.81}Zr_{0.75}(\square)_{0.23}Si_4O_{14}F_{2.72}O_{1.28}$
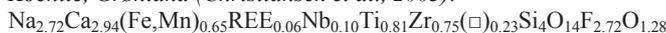
Rosenbuschite-group (?) mineral, LV09, Låven (this work):
$Na_{2.38}Ca_{3.48}(Fe,Mn)_{0.24}REE_{0.17}Nb_{0.06}Ti_{0.74}Zr_{0.86}(\square)_{0.07}Si_4O_{14}F_{3.25}O_{0.75}$
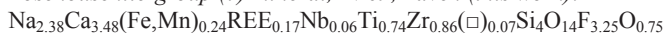
Rosenbushite-group (?) mineral, LV01, Låven (this work):
$Na_{2.51}Ca_{3.11}(Fe,Mn)_{0.46}REE_{0.19}Nb_{0.06}Ti_{0.99}Zr_{0.71}(\square)_{0.0}Si_4O_{14}F_{3.16}O_{0.84}$
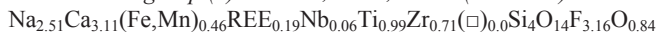
*Rosenbuschite, Langesundsfjord area (Andersen et al. 2010), Ros:
$Na_{2.38}Ca_{3.55}(Fe,Mn)_{0.16}REE_{0.12}Nb_{0.08}Ti_{0.66}Zr_{1.03}(\square)_{0.0}(Si_4O_{14})F_{3.02}O_{0.98}$

*Wöhlerite (Andersen et al. 2010), Woe:
$Na_{2.00}Ca_{3.82}(Fe,Mn)_{0.24}REE_{0.03}Nb_{0.69}Ti_{0.16}Zr_{0.98}(Si_4O_{14})F_{1.79}O_{2.21}$
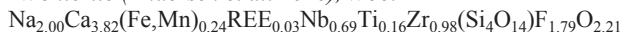
*Hiortdahlite (Andersen et al. 2010), Hio:
$Na_{1.81}Ca_{4.52}(Fe,Mn)_{0.25}REE_{0.09}Nb_{0.12}Ti_{0.09}Zr_{1.13}(Si_4O_{14})F_{3.45}O_{0.55}$

*Låvenite (Andersen et al. 2010), Lav:
$Na_{1.81}Ca_{4.52}(Fe,Mn)_{0.25}REE_{0.09}Nb_{0.12}Ti_{0.09}Zr_{1.13}(Si_4O_{14})F_{3.45}O_{0.55}$
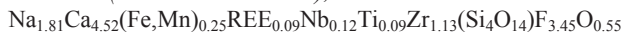
*Astrophyllite, Sagåsen (this work); Ast:
$K_{1.66}Na_{1.01}Ca_{0.23}(Fe,Mn)_{7.00}REE_{0.02}Nb_{0.14}Ti_{1.52}Zr_{0.36}Al_{0.32}Si_{7.74}O_{24}[F_{0.88}(OH)_{3.76}O_{2.36}]$
*Zirconolite (polymignite), Brøgger (1890); Zlt: $Ca_{0.50}REE_{0.50}Fe_{0.60}Nb_{0.40}Zr_{1.00}Ti_{1.00}O_{7.00}$
*Titanite (stoichiometric); Ttn: $CaTiSiO_5$
*Lorenzenite (stoichiometric); Lor: $Na_2Ti_2Si_2O_9$
*Aenigmatite (stoichiometric): $Na_2Fe_5TiSi_6O_{20}$
*Parakeldyshite (stoichiometric): $Na_2ZrSi_2O_7$
*Eudialyte[1]: Eud: $Na_{10.5}K_{0.2}Ca_{6.9}(Fe,Mn)_{3.6}REE_{0.6}Nb_{0.4}Ti_{0.1}Zr_{3.1}Al_{0.1}Si_{25.4}O_{75}F_{0.2}Cl_{1.1}(OH)_2$
*Albite; Ab: $NaAlSi_3O_8$
*K-feldspar; Kf: $KAlSi_3O_8$
*Nepheline; Ne: $Na_3KAl_4Si_4O_{16}$
*Biotite (hydroxy annite);Ann_{bi}: $KFe_3AlSi_3O_{10}(OH)_2$
*Hedenbergite component in aegirine-augite; Hd_{cpx}: $CaFeSi_2O_6$
*Pyrochlore; Pcl: $NaCaNb_2O_6F$
*Fluorite; Flu: CaF_2
*Villiaumite; Vil: NaF
*Sodalite; Sod: $Na_4Al_3Si_3O_{12}Cl$

*: Phase compositions used in chemographic modelling, with abbreviations used in Table 5 and in the text.
1: Data from Andersen et al. (2010)

Ideally, the Ti- and Zr minerals should be part of a single petrogenetic grid (Marks et al. 2010). For this to be of any use, more detailed information is needed on coexisting mineral assemblages in Stavern and Sandefjord suite pegmatites than is currently available. Zr is a minor component in most of the Ti-rich minerals in the pegmatites, and Ti in the Zr minerals; only zirconolite and the rosenbuschite-group minerals have both Ti and Zr as major components. Considering the Zr- and Ti-rich mineral assemblages as two semi-independent sub-systems that mutually control each other's minor components by external buffering is a useful approximation that will be applied here. The ZrO_2 or $ZrSiO_4$ component in Ti-rich mineral assemblages is assumed to be buffered by the Zr-rich minerals, in the same manner as TiO_2 was externally buffered in the Zr-rich mineral assemblages (Andersen et al. 2010). In the zircon-saturated, miaskitic case $a_{ZrSiO4} = 1$; in agpaitic systems, the activity will deviate from unity, but will still be controlled by the zirconium-bearing minerals coexisting with the Ti-minerals but not explicitly involved in reactions.

Zirconolite in these rocks is the REE and Nb enriched mineral species called polymignite by Berzelius (1824); we use a composition $Ca_{0.5}REE_{0.5}Fe_{0.6}Nb_{0.4}ZrTiO_7$ based on analyses by Brøgger (1890). For titanite, parakeldyshite, lorenzenite and aenigmatite, we use ideal endmember compositions; for lorenzenite and parakeldyshite, this is justified by published electron microprobe analyses (Raade, Mladeck 1977; Larsen et al. 1992). Astrophyllite is represented by the average composition from the Sagåsen pegmatite, mosandrite by data from the present study (Table 3) and rinkite by the new analysis of the "jonstrupite" type material by Bellezza et al. (2009b). Rinkite and hainite are close to each other in composition, and the stability fields in activity space are likely to show considerable overlap; we use the rinkite analysis by Bellezza et al. (2009b) to represent both in our model.

By including villiaumite (*Vil*, NaF) as a phase, the analysis can be extended towards hyperagpaitic compositions. We are, however, not aiming for a chemographic analysis of hyperagpaitic magmas, for which a number of minerals that are not relevant to the LPC should be included (e.g. ussingite, natrosilite, zirsinalite etc., e.g. Khomyakov 1995). Divariant reactions involving parakeldyshite and Ti-rich minerals have been balanced by matrix inversion using built-in functions of Microsoft Excel (Table 5). Reactions involving Zr-dominated species other than parakeldyshite were given by Andersen et al. (2010).

TABLE 5

Divariant reactions defining the petrogenetic grid

---

a: Reactions involving parakeldyshite

Pks1 (against Zrc): 1.00 Pks + 0.38 Ab + 0.13 Kf = 1.00 Zrc + 0.13 Ne + Nds

Pks2 (against Eud): 3.06 Pks + 0.38Ab+1.40 Kf + 6.70 Hd$_{cpx}$ + 0.05 TiO$_2$ + 0.22Pcl +
0.30 REE$_2$O$_3$ +1.50 H$_2$O + 2.15Nds + 1.09 HCl = 1.00 Eud + 0.17 Ne +
1.04 Ann$_{bi}$ + 0.02 HF

Pks3 (against Cat): 1.00 Pks + 0.38 Ab + 0.22 Kf + 0.30 Hd$_{cpx}$ +2.10 H$_2$O = 1.00 Cat + 0.12 Ne
+ 0.10 Ann$_{bi}$ +0.30 Nds

Pks4 (against Woe): 0.98 Pks + 0.58 Ne + 0.51 Kf + 3.47 Hd$_{cpx}$+0.16 TiO$_2$+0.34 Pcl + 0.01
REE$_2$O$_3$ + 0.35 H$_2$O + 1.45 HF = 1.00 Woe + 1.73 Ab +1.08 Ann$_{bi}$ +
0.15 Nds

Pks5 (against Hio): 1.13 Pks + 0.83 Ne + 0.57 Kf + 4.46 Hd$_{cpx}$ + 0.09 TiO$_2$ + 0.06 Pcl +
0.04 REE$_2$O$_3$ + 3.39 HF = 1.00 Hio + 2.50 Ab + 1.40 Ann$_{bi}$ + 0.29 H$_2$O +
0.25 Nds

Pks6 (against Ros): 1.03 Pks + 0.67 Ne + 0.45 Kf + 3.51 Hd$_{cpx}$ + 0.66 TiO$_2$ + 0.04 Pcl +
0.06 REE$_2$O$_3$ + 0.13 Nds + 2.98 HF = 1.00 Ros + 2.01 Ab + 1.12 Ann$_{bi}$ +
0.37 H$_2$O

Pks7 (against Lav): 1.64 Pks + 0.29 Ne + 0.02 Kf + 1.72 Hd$_{cpx}$ + 0.29 TiO$_2$ + 0.12 PCl +
0.01 REE$_2$O$_3$ + 2.52 HF = 1.00 Lav + 0.88 Ab + 0.31 Ann$_{bi}$ + 0.95 H$_2$O +
0.20 Nds

---

b: Reactions involving titanium-rich minerals

---

i: Zirconolite (polymignite) volume

Zlt1 (against Aen) 1.00 Zlt + 2.03 Ab + 1.57 Ann$_{bi}$ + 1.10 Nds + 0.20 HF = 1.00 Aen +
1.00 ZrSiO$_4$ + 0.68 Ne + 0.89 Kf + 0.30 Hd$_{cpx}$ + 0.20 Pcl + 0.25
REE$_2$O$_3$+1.67 H$_2$O

Zlt2 (against Lor) 2.00 Zlt +1.05 Ab + 0.55 Kf + 1.20 Nds + 0.40 HF = 1.00 Lor + 2 ZrSiO$_4$ +
0.35 Ne + 0.20 Ann$_{bi}$ + 0.60 Hd$_{cpx}$ + 0.40 Pcl + 0.50 REE$_2$O$_3$

Zlt3 (against Ast) 1.52 Zlt + 0.90 Ab + 0.28 Kf + 2.13 Ann$_{bi}$ + 1.29 Nds + 1.11 HF = 1.00 Ast
+ 1.16 ZrSiO$_4$ + 0.75 Ne + 0.30 Hd$_{cpx}$ +0.23 Pcl + 0.37 REE$_2$O$_3$+ 0.80 H$_2$O

Zlt4 (against Ttn) 1.00 Zlt + 0.15 Ab + 0.70 Hd$_{cpx}$ +0.33 H$_2$O + 0.10 Nds + 0.20 HF = 1.00 Ttn
+ 1.00 ZrSiO$_4$ + 0.05 Ne + 0.43 Ann$_{bi}$ + 0.20 Pcl + 0.25 REE$_2$O$_3$

ii: Astrophyllite volume

Ast1 (against Aen) 0.66 Ast + 1.43 Ab + 0.17 Ann$_{bi}$ + 0.25 Nds = 1.00 Aen + 0.24 ZrSiO$_4$ +
0.18 Ne + 1.07 Kf + 0.10 Hd$_{cpx}$ + 0.05 Pcl + 0.01 REE2O3 + 1.14 H2O +
0.53 HF

Ast2 (against Lor) 1.32 Ast + 0.63 Ne + 0.19 Kf + 1.06 H$_2$O = 1.00 Lor + 0.48 ZrSiO$_4$ +
0.13 Ab + 3 Ann$_{bi}$ + 0.20 Hd$_{cpx}$ + 0.10 Pcl + 0.01 REE$_2$O$_3$ + 0.50 Nds +
1.06 HF

Ast3 (against Ttn) 0.66 Ast + 0.44 Ne + 0.30 Kf + 0.90 Hd$_{cpx}$ + 0.86 H$_2$O = 1.00 Ttn +
0.24 ZrSiO$_4$+ 0.44 Ab + 1.83 Ann$_{bi}$ + 0.05 Pcl + 0.01 REE$_2$O$_3$ + 0.75 Nds +
0.53 HF

Ast4 (against Rin) 0.47 Ast + 1.03 Ne + 0.63 Kf + 4.10 Hd$_{cpx}$ + 0.36 REE$_2$O$_3$ + 0.81 H$_2$O +
0.48 Nds + 2.40 HF = 1.00 Rin + 0.08 ZrSiO$_4$ + 2.47 Ab + 2.44 Ann$_{bi}$

iii: Rinkite / hainite volume

Rin1 (against Lor)* 2.82 Rin + 6.83 Ab + 3.87 Ann$_{bi}$ = 1.00 Lor + 0.25 ZrSiO$_4$ + 2.28 Ne +
1.60 Kf + 11.76 Hd$_{cpx}$ + 0.10 Pcl + 1.03 REE$_2$O$_3$ + 1.22 H$_2$O + 1.85 Nds +
7.82 HF

Rin2 (against Ttn)	1.41 Rin + 3.04 Ab + 1.60 Ann$_{bi}$ = 1.00 Ttn + 0.13 ZrSiO$_4$ + 1.01 Ne + 0.59 Kf + 4.88 Hd$_{cpx}$ + 0.05 Pcl + 0.51 REE$_2$O$_3$ + 0.28 H$_2$O + 1.43 Nds + 3.91 HF
Rin3 (against Mos)	1.32 Rin + 1,82 Ab + 0.62 Ann$_{bi}$ + 0.05 REE$_2$O$_3$ + 3.79 H$_2$O = 1.00 Mos + 0.02 ZrSiO$_4$ + 0.61 Ne + 0.02 Kf + 1.83 Hd$_{cpx}$ + 1.21 Nds + 2.78 HF
iv: Mosandrite volume	
Mos1 (against Lor)	2.14 Mos + 2.94 Ab + 2.54 Ann$_{bi}$ + 0.74 Nds = 1. 00 Lor + 0.21 ZrSiO$_4$ + 0.98 Ne + 1.56 Kf + 7.83 Hd$_{cpx}$ + 0.09 Pcl + 1.14 REE$_2$O$_3$ + 9.33 H$_2$O + 1.87 Hf
Mos2 (against Ttn)	1.07 Mos + 1.09 Ab + 0.94 Ann$_{bi}$ = 1.00 Ttn + 0.11 ZrSiO$_4$ + 0.36 Ne + 0.57 Kf + 2.92 Hd$_{cpx}$ + 0.05 Pcl + 0.57 REE$_2$O$_3$ + 4.33 H$_2$O + 0.13 Nds + 0.94 HF
Mos3 (against Ast)	1.63 Mos + 0.20 ZrSiO$_4$ + 2.33 Ab + 4.21 Ann$_{bi}$ + 0.94 Nds = 1.00 Ast + 1.23v Ne + 1.33 Kf + 5.80 Hd$_{cpx}$ + 0.85 REE$_2$O$_3$ + 7.90 H$_2$O + 0.62 HF
v: Aenigmatite-lorenzenite	
Lor1	2.00 Aen + 1.00 Ne + 2.33 Kf + 3.33 H$_2$O = 1.00 Lor + 3.00 Ab + 3.33 Ann$_{bi}$ + 1.00 Nds
c: Other reactions	
Fluorite saturation	0.35 Ne + 0.08 Kf + Hd$_{cpx}$ + 2HF = 1.00 Flu + 0.75 Ab + 0.33 Ann$_{bi}$ + 0.67 H$_2$O
Villiaumite saturation	0.13 Ne + 0.5 Nds + 1.00 Hf = 1.00 Vil + 0.38 Ab + 0.13 Kf + 0.50 H$_2$O

5.1. Eudialyte

Eudialyte is the most common indicator mineral for agpaitic rocks in general, and in many agpaitic complexes it is the main zirconium-bearing mineral (e.g. Sørensen 1997). The pegmatites in the LPC are special in that other Zr-bearing minerals are equally abundant. The stability field of eudialyte in *log a$_{Nds}$ – log a$_{H2O}$ - log a$_{HF}$* space is situated at high *a$_{Nds}$*, and since the minerals of the eudialyte group contain essential Cl$^-$, the size of the stability volume for eudialyte will be dependent on the chlorine (or HCl) activity in addition to alkalinity; the minimum *a$_{Nds}$* compatible with stable eudialyte decreases with increasing *a$_{HCl}$*. The maximum attainable *a$_{HCl}$* (and thereby the maximum stability range of eudialyte) is found in magmas crystallizing nepheline + sodalite (Andersen et al. 2010). In Figure 6a, the stability field of eudialyte is shown at *a$_{HCl}$* less than this maximum value, in order to accommodate parakeldyshite-catapleiite-zircon assemblages in the Bratthagen suite pegmatites.

5.2. Fluorite and villiaumite saturation

The maximum HF activity attainable is given by saturation of the magma with fluoride minerals. In mildly agpaitic magmas, fluorite will form (Andersen et al. 2010), whereas villiaumite may precipitate in hyperagpaitic magmas. The saturation planes for fluorite and villiaumite are divariant in activity space (Fig. 6). Since there is no evidence of villiaumite or other hyperagpaitic mineral assemblages in the LPC, the *Vil+Flu* univariant defines a maximum limit for *a$_{Nds}$* under fluorite-saturated conditions.
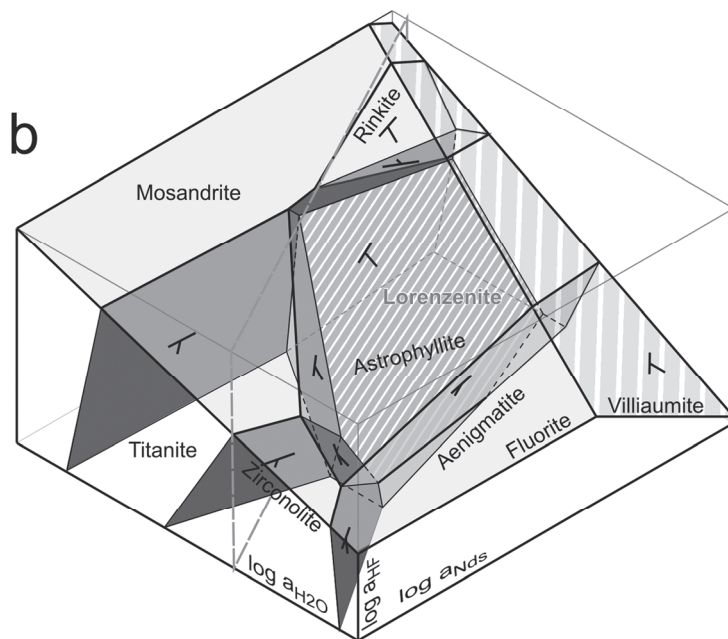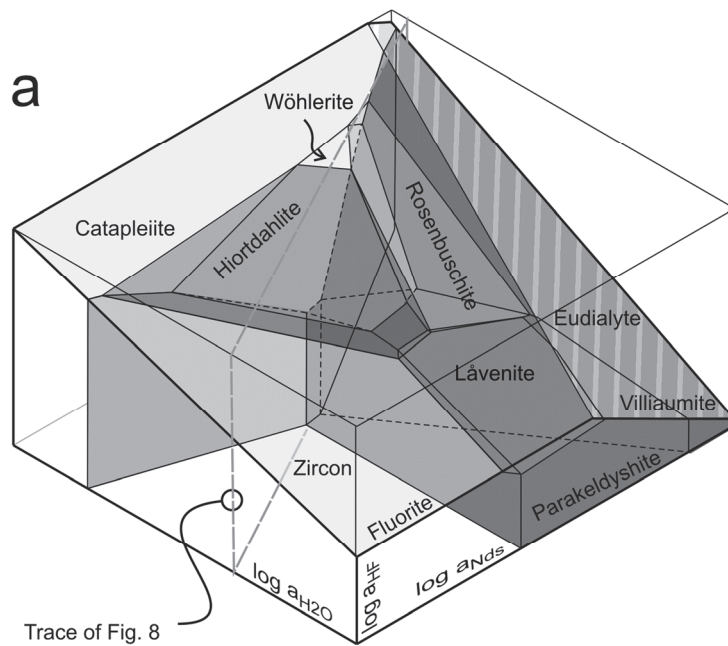
Fig. 6. 3D view of the petrogenetic grids for (a): Zr-rich minerals and (b): Ti rich minerals. The grid in (a) is drawn at a_{HCl} lower than maximum (see Fig. 7 in Andersen et al. 2010), and is modified from the grid in Andersen et al. (2010) to incorporate a stability volume for parakeldyshite.

5.3. Parakeldyshite in the Bratthagen suite pegmatites

As a volatile-free zirconium silicate mineral, parakeldhyshite (*Pks*, $Na_2ZrSi_2O_7$) is expected to be stable at low a_{HF} and a_{H2O}. Its stability volume in $log\ a_{Nds} - log\ a_{H2O} - log\ a_{HF}$ space is limited against the volumes of zircon (*Zrc*), eudialyte (*Eud*) and catapleiite (*Cat*) by reactions Pks1, Pks2 and Pks3, respectively (Table 5a). These reactions are insensitive to a_{HF}, and define a wedge-shaped volume (Fig. 6a) whose extent in a_{Nds} direction depends on the size of the eudialyte volume, which in turn depends on the HCl activity (Andersen et al. 2010). The presence of parakeldyshite with zircon and catapleiite in the Bratthagen pegmatites suggests the presence of a *Zrc + Pks + Cat* univariant, and a *Pks + Cat* divariant at fluorite-undersaturated conditions (Fig. 6a). Towards high a_{HF}, the parakeldyshite volume is limited by stability volumes of låvenite (*Lav*), hiortdahlite (*Hio*), wöhlerite (*Woe*) and rosenbuschite (*Ros*), and it will reach fluorite or villiaumite saturated conditions only at elevated a_{Nds}, at or approaching hyperagpaitic conditions, and then only in systems where eudialyte does not form because of low a_{HCl} or other causes. Thus, the elevated HF activity is the main reason for the absence of parakeldyshite from the Langesundsfjord suite pegmatites – in low a_{H2O} systems, such as the "dry" parts of the Låven pegmatite, låvenite will form instead of parakeldyshite (Fig. 6a).

5.4. Ti-rich minerals in miaskitic and agpaitic pegmatites

Divariant reactions limiting the stability fields of zirconolite (*Zlt*), titanite (*Ttn*), lorenzenite (*Lor*), aeningmatite (*Aen*), astrophyllite (*Ast*), rinkite (*Rin*) and mosandrite (*Mos*) are given in Table 5b. To construct a 3D petrogenetic grid for these minerals compatible with the grid for Zr-rich minerals, it is assumed that the stability volumes for zirconolite and titanite will overlap the zircon volume, that the mosandrite volume will overlap with that of catapleiite, and rinkite/hainite with rosenbuschite. Most of the divariant reactions are less dependent on a_{HF} than those in the Zr-dominated system, the astrophyllite – lorenzenite reaction (Ast2) is an exception, with astrophyllite at the low a_{H2O} – high a_{HF} side (Fig. 6, 7). The lorenzenie volume will therefore be more or less covered by the astrophyllite volume, and may potentially reach the fluorite saturation plane only at elevated a_{H2O}, in which case a *Lor+Flu* field will suppress the *Mos+Ttn+Ast+Flu* invariant (and possibly also *Mos+Rin+Ast+Flu*) in Figure 7. In the LPC pegmatites, magmatic lorenzenite has only been reported from the fluorite-undersaturated B1 assemblage at Bratthagen, and it is therefore suggested that the lorenzenite volume will not reach the fluorite saturation plane at the prevailing P and T.
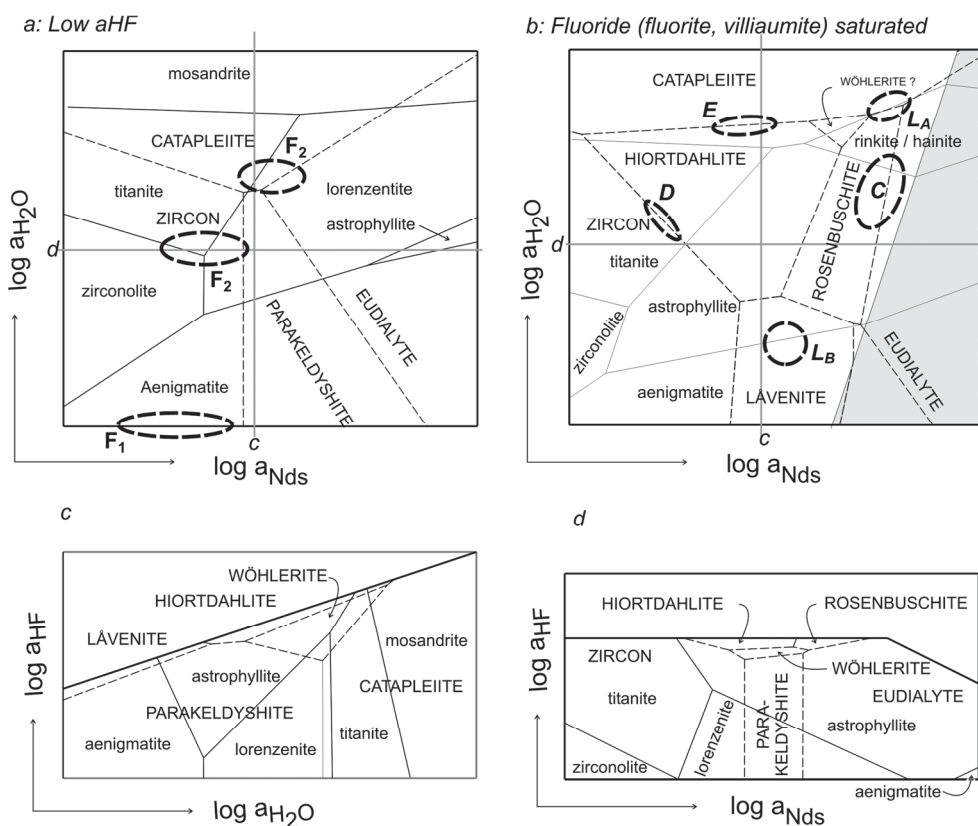
Fig. 7. Superposed sections of the grids for Ti- (*continuous lines, lower case*) and Zr-rich minerals (*broken lines, upper case*). The eudialyte field has been drawn at lower a_{HCl} than the saturation limit for sodalite inferred by Andersen et al. (2010), in order to allow a possible parakeldyshite+zircon+catapleiite assemblage in the Bratthagen suite pegmatites. Circles with heavy, broken outlines are the activity relationships indicated by critical mineral assemblages in the LPC pegmatites, see Table 2 for identification of assemblages and the text for further explanation, Figure 8 gives further details.

a: Section parallel to the log a_{Nds} and log a_{H2O} axes at low a_{HF}, corresponding to the bottom face of the 3D diagrams in Figure 6. Note the large stability fields of lorenzenite and parakeldyshite at these conditions.

b: Projection of the fluoride-saturation plane onto the *log a_{Nds}* - *log a_{H2O}* plane. Within the grey field, villiaumite rather than fluorite is the stable fluoride mineral, a condition not reached in the LPC pegmatites. In a system saturated with fluorite, the parakeldyshite and lorenzenite stability fields have disappeared, and the wöhlerite field is small or non-existent (see discussion in the text, and Andersen et al. (2010) for a discussion of the possible stability of wöhlerite + fluorite).

c: log a_{H2O}-log a_{HF} section at constant a_{Nds} along line c in Figure 7a and b. The heavy line is the intersection with the fluorite saturation plane, representing the maximum a_{HF} attainable in the system. Note that the stability fields of parakeldyshite, wöhlerite and lorenzenite will not reach the fluorite saturation plane

d: log a_{Nds} − log a_{HF} section at constant a_{H2O}, along the line marked d in Figure 7a and b. The heavy line is the intersection with the fluorite (horizontal) and villiaumite (sloped) saturation planes. Note

that the lorenzenite field rapidly disappears at increasing a_{Nds}. Neither this, nor the fields of wöhlerite and parakeldyshite will reach fluoride-saturated conditions along this transect.

At low a_{H2O}, the grid is dominated by volumes for zirconolite (at low a_{Nds}) and aenigmatite, neither of which is strongly sensitive to a_{HF}. Titanite is stable at higher a_{H2O} and low a_{Nds}, whereas the stability field of astrophyllite spans a large range of a_{Nds}, ranging from miaskitic conditions with zircon to hyperagpaitic with villiaumite. Mosandrite is stable at high a_{H2O}, and is relatively insensitive to both a_{Nds} and a_{HF}. Assuming the existence of a stable *Ast+Mos+Flu* assemblage, corresponding to the situation in the "wet" parts of the Låven pegmatite, the rinkite / hainite field is restricted to a volume at or close to fluorite saturation at elevated a_{Nds} and a_{H2O}, limited against the astrophyllite and mosandrite fields by shallow-dipping divariant planes.

6. Discussion

6.1. The "pegmatite magma"

The LPC pegmatites have crystallized from highly evolved magmas that were rich in volatile components and in incompatible elements (Neumann 1980). From mineralogical similarities between pegmatite and larvikite, it has generally been accepted that the miaskitic pegmatites of the Stavern suite, and at least some of the pegmatites in the Sandefjord suite are genetically related to their host larvikite (Brøgger 1890; Dahlgren 2010; Larsen 2010). In the case of the Bratthagen suite, there is compelling field and mineralogical evidence that they have formed from residual liquids derived from a local nepheline syenite precursor (Sæbø 1966; Dahlgren 2010). The nepheline syenite pegmatites of the Langesundsfjord suite differ from the larvikite of ring segment VI in terms of mineralogy and chemical composition. Some of these pegmatites are spatially associated with nepheline syenite intrusions in larvikite (e.g. the Sagåsen pegmatite), and non-pegmatitic, miaskitic to mildly agpaitic nepheline syenite intrusions occur in the south-western border region of ring segment VI (Dahlgren 2010). Both of these pegmatite suites may therefore have been derived from liquids generated by shallow or even in-situ fractional crystallization of a peralkaline nepheline syenite magma, rather than a less alkaline and less silica undersaturated larvikite magma. The nepheline syenite intrusions crosscutting the LPC and the larvikite itself may represent semi-parallel fractionation trends of a common parental magma at mid- to deep crustal levels (Neumann 1980).

6.2. Contrasting crystallization conditions of LPC pegmatites

The most common Ti and Zr bearing minerals in the LPC larvikites are ilmenite, titanomagnetite, titanite and zircon, i.e. a typical miaskitic mineral assemblage; this applies to nepheline-bearing as well as to nepheline-free varieties (Neumann 1980). Titanite does occur in the Stavern suite pegmatites, but it is not very abundant, and in some pegmatites it is a secondary rather than primary magmatic mineral (Larsen 2010).

A zirconolite-bearing mineral assemblage would in general suggest a lower silica activity than one with zircon and/or titanite. It is thus possible that the change from a normal zircon + titanite assemblage to one with zirconolite ± zircon (varieties of

assemblage M_1, Table 2, Fig. 8) is a result of increasing degree of silica undersaturation during the final, shallow-level fractionation of the larvikite magma envisaged by Neumann (1980). It should, however, be noted that the zirconolite forming in these pegmatites is quite far from a simple $CaTi_2ZrO_7$ composition. 50% of the titanium is replaced by Nb and REE, and it is possible that an increase in these elements during fractional crystallization is the decisive factor stabilizing zirconolite.
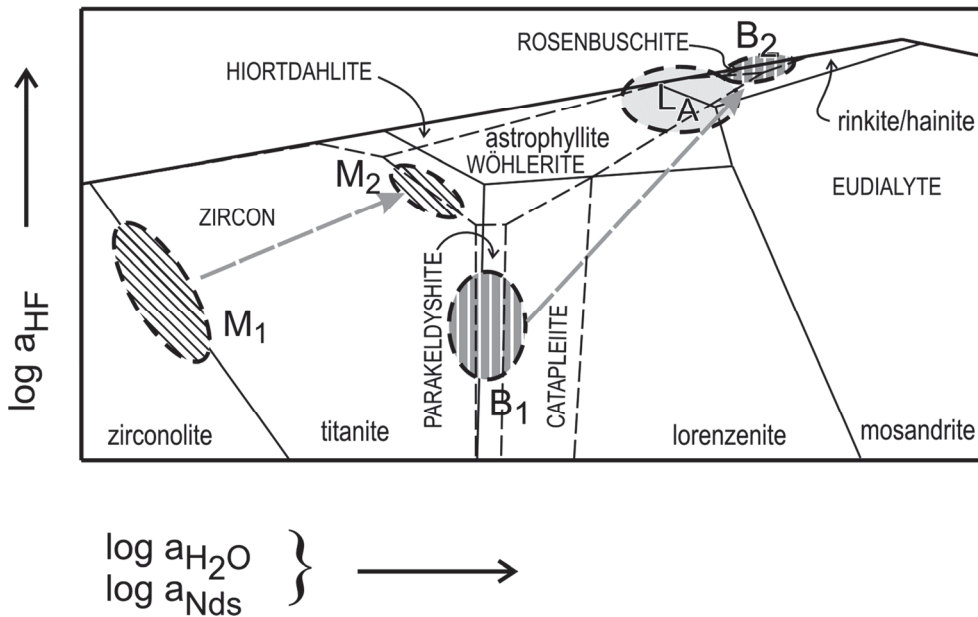

Fig. 8. Diagonal section parallel to the a_{HF} axis through the 3D petrogenetic grids along the broken lines in Figure 6. Stability fields for Ti- (*broken lines, lower case*) and Zr-rich minerals (*continuous lines, upper case*) have been superposed. Going from left to right along this transect, a_{H2O} and a_{NdS} will increase in parallel. Circles with heavy, broken outlines are the activity relationships indicated by critical mineral assemblages in the LPC pegmatites, see Table 2 for identification of assemblages and the text for further explanation. The broken arrows represent trends of increasing a_{HF}, a_{H2O} and a_{Nds} with time, interpreted as a result of in-situ fractionation of volatile-free minerals from the pegmatite magma.

Regardless of the reason for its presence, high-Nb-REE zirconolite would be a stable phase only at low a_{Nds} and low to moderate a_{H2O}. The effect of fluorine on zirconolite stability is moderate, but the size of the stability field will expand towards lower a_{HF} (Fig. 7). Wöhlerite has been reported from a few of the Stavern suite pegmatites in the eastern part of the LPC (the M_2 assemblage). This suggests parallel increases in Nds, water and HF, causing a trend towards agpaitic conditions, but not sufficiently to reach fluorite saturation (Fig. 8). The cause of this could be in-situ fractionation of alkali feldspar from a peralkaline pegmatite magma.

The Bratthagen pegmatites show a very distinct, early mineral assemblage with parakeldyshite, zircon, lorenzenite and catapleiite. Whether or not all of these are in mutual

equilibrium, the B_1 assemblage points to a restricted volume within the fluorite-undersaturated part of the petrogenetic grid centred on the *Zrc+Cat+Pks* univariant (Fig. 6, 7). Like in the Stavern suite, the subsequent evolution of the Bratthagen magma consists of parallel increases in water, HF and Nds activity, but in this case terminating at the fluorite saturation surface (B_2 assemblage, Fig. 8). Eudialyte is present as a late magmatic mineral in this pegmatite, suggesting that the magma has encountered an eudialyte-in reaction at or near fluorite saturation, and that this has prevented further development towards high a_{Nds} and hyperagpaitic conditions.

The evolution of the Langesundsfjord suite was studied by Andersen et al. (2010). A common feature for these pegmatites is a main stage of magmatic crystallization at fluorite-saturated conditions, but at different a_{H2O} and a_{Nds} conditions, probably controlled by local crystallization trends or local differences in magma compositions. Zirconium silicate assemblages forming at this stage include *Zrc+Hio+Flu, Hio+Cat+Flu, Lav+Flu, Hio+Ros+Flu±Eud* (assemblages D, E, L_B and C in Table 2b and Fig. 7b). A common feature is an evolution at increasing a_{HF}, leading from wöhlerite- to fluorite-bearing assemblages with time. Several of the pegmatites studied by Andersen et al. (2010) crystallized near the intersection of the *Hio+Ros+Flu* univariant with the maximum extent of the eudialyte field. Figure 6b suggests that astrophyllite would be the stable Ti silicate mineral under these conditions, in good agreement with the abundance of astrophyllite in this suite of pegmatites (Fig. 2b). Relatively small increases in a_{H2O} at fluorite saturation would, however, stabilize either rinkite/hainite, or mosandrite in these pegmatites.

The nepheline syenite of the boundary zone of the Sagåsen pegmatite shows a shift from a transitional assemblage with zircon and wöhlerite to one with rosenbuschite, hainite and fluorite, possibly related to fluids emanated from the pegmatite (assemblages SC_1 to SC_2, Table 2b, Fig. 8). Again, parallel increases in a_{Hf}, a_{H2O} and a_{Nds} are involved (Fig. 8). The evolution from S1 to S2 in the Sagåsen pegmatite is an example of a different type of trend, from highly alkaline (S1) to less alkaline, but still mildly agpaitic conditions (assemblage S2 in Table 2b and Fig. 7d). A similar low-alkali trend with late magmatic hiortdahlite + zircon + fluorite forming after wöhlerite-bearing assemblages was seen in one of the Langesundsfjord suite pegmatites studied by Andersen et al. (2010; assemblages a_1 and a_2 in the Langodden pegmatite).

The Sandefjord suite of pegmatites probably represents several different lines of magmatic evolution, in which both the starting composition and the evolutionary mechanisms may be different. Some of the pegmatites are quartz syenitic (Larsen 2010), in which case a chemographic analysis assuming silica-undersaturation cannot be directly applied. One feature that seems to be common in these pegmatites is the early crystallization of aenigmatite, indicating dry conditions (assemblage F_1, Table 2d, Fig. 7a). Zirconolite, catapleiite, eudialyte and astrophyllite (assemblage F_2, Table 2d, Fig. 7a) have been reported from different occurrences in the area. This suggests a general trend of evolution towards increasing water activity, but at different a_{Nds} (Fig. 7a), perhaps a number of parallel trends locally controlled by the in-situ growth of anhydrous, mildly peralkaline mineral assemblages (alkali feldspar +sodic pyroxene), which would prevent large excursions in a_{Nds} during evolution. Fluorite has been reported from only one of the aenigmatite-bearing pegmatites in the eastern area (Fig. 2b). Although this may be a question as much of the absence of observations as of the absence of the mineral, it could

suggest that growth of fluorine-bearing silicate minerals (amphibole ?) kept the HF activity down during in-situ evolution, and thereby prevented the type of evolution seen in the Langesundsfjord suite.

6.3. The role of astrophyllite

The members of the wöhlerite and rosenbuschite mineral groups show little internal compositional variation, due to rigid structure types in which a small chemical change would induce a new configuration of coordination polyhedra and thereby stabilize another mineral species. The simple identification of minerals such as wöhlerite, hiortdahlite or låvenite can therefore give important information on the crystallization conditions even without chemical analysis of the individual phases. In contrast, the stability volume of astrophyllite spans large ranges in all three activity variables considered here, from miaskitic to hyperagpaitic conditions (Fig. 6, 7). The presence of astrophyllite in an alkaline rock is therefore not sufficient to classify the rock as agpaitic; for that purpose, information on the accompanying, Zr-rich minerals is needed. What the presence of astrophyllite does convey is that the water activity of the magma was "intermediate" between dry magmas crystallizing aenigmatite or låvenite, and water-rich magmas crystallizing catapleiite ± mosandrite.

6.4. Mosandrite, catapleiite and high-water agpaitic system

Mosandrite and catapleiite are stable only at elevated water activity. The presence of aqueous (?) fluid inclusions in catapleiite (Brøgger 1890; Andersen et al. 2010) suggests that these minerals have crystallized in the presence of a free fluid phase, i.e. the magma was saturated in water. Both of these minerals were first described from the Låven pegmatite (Erdmann 1840; Weibye 1850). The distribution of minerals in the Låven pegmatite is far from homogeneous, and mosandrite is concentrated in "nests" near the top of the present exposures (Larsen 2010). The contrasting mineralogy points to lack of wide-ranging equilibrium in this pegmatite, and large contrasts of water activity in either time, space or both. One way of producing this pattern would be by intrusion of separate batches of nepheline syenite magma with different water contents. Another, and perhaps more likely, mechanism is exsolution and migration of an aqueous fluid during in-situ crystallization. Separation of an aqueous fluid from the magma will in itself not explain the contrasting mineral assemblages, since the fluid would initially be saturated in the same solid phases as the silicate melt from which it separated. However, a scenario with contrasting "dry" and "wet" domains may be established if the fluid phase is able to migrate through the partly crystallized mush, reacting with melt and solids along the way. The aqueous fluid would eventually concentrate under the roof of the intrusion, or in other favourable traps within the body of the pegmatite.

7. Conclusions

Based on a chemographic analysis of mineral assemblages in pegmatites related to the Larvik Plutonic Complex in the Oslo Rift, it is possible to construct semiquantitative

isobaric-isothermal petrogenetic grids relating the stability of Ti- and Zr- rich mineral assemblages to the activities of $Na_2Si_2O_5$ (*Nds*), H_2O and HF in highly evolved, residual magmas in the complex. The Ti-silicate mineral assemblages are less sensitive to fluoride activity than the associated Zr silicates. The exception is lorenzenite, which is stable at low HF activity, i.e. at fluorite undersaturated conditions. Astrophyllite is stable over wide ranges of both alkali and fluoride activity, ranging from miaskitic to hyperagpaitic conditions, but is unstable at both very dry and water-saturated conditions. On the other hand, mosandrite and catapleiite are characteristic of high water activity, including water-saturated systems.

Based on the distribution of Ti- and Zr rich magmatic minerals, it is possible to define at least four different suites of pegmatites in the complex. Miaskitic, syenite pegmatites with or without nepheline carry zircon and Nb-REE-Fe rich zirconolite (polymignite) as characteristic minerals. These pegmatites (the Stavern suite) formed at low a_{Nds} and relatively dry conditions; the stability of zirconolite in these pegmatites is not strongly dependent on the activity of HF. Some of these pegmatites evolve towards mildly agpaitic compositions, with wöhlerite-bearing mineral assemblages. More strongly peralkaline residual magmas form a suite of mildly agpatic pegmatites with eudialyte, astrophyllite and members of the rosenbuschite and wöhlerite groups as characteristic minerals (the Langesundsfjord suite). These pegmatites formed at Nds activity distinctly higher than the miaskitic pegmatites, and at a_{HF} levels corresponding to fluorite saturation during the main phase of magmatic crystallization, but at variable a_{H2O}. In some of these pegmatites, contrasting "dry", låvenite-bearing and "wet" mosandrite + catapleiite bearing assemblages can be found, for example in the Låven pegmatite, suggesting exsolution and migration of an aqueous fluid during magmatic crystallization. Rare parakeldyshite-lorenzenite bearing pegmatites make up a distinct group (the Bratthagen suite), which differs from the Langesundsfjord suite pegmatites mainly in low a_{HF} during the main stage of magmatic crystallization. The minerals lorenzenite and parakeldyshite will normally not coexist with fluorite; at elevated a_{HF}, they will be replaced by astrophyllite and låvenite, respectively. The HF activity increased during crystallization, forming a late-stage rosenbuschite-fluorite-eudialyte assemblage similar to the Langesundsfjord suite. A fourth group of pegmatites (the Sandefjord suite) is transitional between miaskitic and agpaitic compositions, and reflects more than one trend of in-situ evolution of residual magmas from dry conditions (characterized by aenigmatite) to assemblages with astrophyllite, eudialyte and zirconolite.

The present results support the traditional idea that increasing peralkalinity (i.e. increasing a_{Nds}) is an important driving force for the transition from miaskitic to agpaitic mineral assemblages crystallizing from a nepheline syenitic magma. However, the actual Ti-Zr silicate liquidus mineralogy of the pegmatite magma will be controlled by components such as water, chlorine and, in particular, fluorine.

are due to Hans Jørgen Berg for assistance with XRD analysis, to Berit Løken Berg for assistance with the scanning electron microscope and to Siri Simonsen for preparing polished microprobe mounts. The manuscript has benefited from the helpful comments of two anonymous reviewers.

8. References

Andersen, T., Erambert, M., Larsen, A.O., & Selbekk, R.S. (2010). Petrology of nepheline syenite pegmatites in the Oslo Rift, Norway: Zirconium silicate mineral assemblages as indicators of alkalinity and volatile fugacity in mildly agpaitic magma. *Journal of Petrology, 51*(11), 2303-2325. DOI: 10.1093/petrology/egq058

Bellezza, M., Merlino, S., & Perchiazzi, N. (2009a). Mosandrite: Structural and crystal-chemical relationships with rinkite. *The Canadian Mineralogist, 47*, 897-908. DOI: 10.3749/canmin.47.4.897

Bellezza, M., Merlino, S., Perchiazzi, N., & Raade, G. (2009b). "Johnstrupite": A chemical and structural study. *Atti della Società toscana di Science naturali Serie A, 114*, 1-3.

Berthelsen, A., Olerud, S., & Sigmond, E.M.O. (1996). *Geologisk kart over Norge, bergrunnskart OSLO 1: 250 000*. Norges geologiske undersøkelse, Trondheim

Berzelius, J. (1824). Undersökning af några Mineralier. 2. Polymignit. *Kungliga Svenska Vetenskaps-Akademiens Handlingar, 1824*, 338-345.

Brøgger, W.C. (1890). Die Mineralien der Syenitpegmatitgänge der südnorwegischen Augit- und Nephelinsyenite. *Zeitschrift für Krystallographie, 16*, 1-235 + 1-663.

Christiansen, C.C., Johnsen, O., & Makovicky, E. (2003). Crystal chemistry of the rosenbuschite group. *The Canadian Mineralogist, 41*, 1203-1224.

Dahlgren, S. (2010). The Larvik Plutonic Complex: The larvikite and nepheline syenite plutons and their pegmatites. In A.O. Larsen (Ed). *The Langesundsfjord. History, Geology, Pegmatites, Minerals (*pp. 26-37*)*. Salzhemmendorf, Germany: Bode Verlag GmbH,

Dons, J.A., & Jorde, K. (1978). *Geologisk kart over Norge, bergrunnskart SKIEN 1: 250 000.* Norges geologiske undersøkelse, Trondheim.

Erdmann, A. (1840). Undersøkning av Leukophan, ett nytt mineral från trakten av Brewig i Norige. *Kungliga Svenska Vetenskaps-Akademiens Handlingar, 1840*, 191-200.

Jarosewich, E. & Boatner, L.A. (1991). Rare-earth element reference samples for electron microprobe analysis. *Geostandards Newsletter, 15*, 397-399.

Johnsen, O., Ferraris, G., Gault, R.A., Grice, J.D., Kampf, A.R., & Pekov, I.V. (2003). The nomenclature of eudialyte-group minerals. *The Canadian Mineralogist, 41*,785-794.

Khomyakov, A.P., (1995). *Mineralogy of hyperagpaitic alkaline rocks.* Oxford and New York: Clarendon Press, Oxford.

Larsen, A.O. (2010). The Langesundsfjord. History, Geology, Pegmatites, Minerals. Salzhemmendorf, Germany: Bode Verlag GmbH.

Larsen, A.O., Raade, G., & Sæbø, P.C. (1992). Lorenzenite from the Bratthagen nepheline syenite pegmatites, Lågendalen, Oslo Region, Norway. *Norsk Geologisk Tidsskrift, 72*(4), 381-384.

Larsen, A.O., Åsheim, A., & Gault, R.A. (2005). Minerals of the eudialyte group from the Sagåsen larvikite quarry, Porsgrunn, Norway. *Norsk Bergverksmuseets skriftserie*, *30*, 58-62.

Larsen, B.T., Olaussen, S., Sundvoll, B., & Heeremans, M. (2008). The Permo-Carboniferous Oslo Rift through six stages and 65 million years. *Episodes, 31*(1), 52-58.

Liestøl, G.B. (1956). *Noen petrografiske og mineralogiske undersøkelser omkring pegmatittgangene i Langesundsfjorden.* Unpublished MSc thesis, University of Oslo, Oslo, Norway.

Marks, M.A.W., Hettmann, K., Schilling, J., Frost, B.R., & Markl, G. (2011). The mineralogical diversity of alkaline igneous rocks: critical factors for the transition from miaskitic to agpaitic phase assemblages. *Journal of Petrology, 52*(3), 439-455. DOI: http://dx.doi.org/10.1093/petrology/egq086

Murad, E. (2006). Mineralogy of aegirine from Låven island, Langesundsfjorden, southern Norway. *Norwegian Journal of Geology, 86*, 435-438.

Neumann, E.-R. (1976). Compositional relations among pyroxenes, amphiboles and other mafic phases in the Oslo Region plutonic rocks. *Lithos 9*(2)*,* 85-109. DOI: http://dx.doi.org/10.1016/0024-4937(76)90028-1

Neumann, E.-R. (1980). Petrogenesis of the Oslo Region larvikites and associated rocks. *Journal of Petrology, 21*, 498-531.

Neumann, E.-R., Wilson, M., Heeremans, M., Spencer, E.A., Obst, K., Timmerman, M.J., & Kirstein, L. (2004). Carboniferous-Permian rifting and magmatism in southern Scandinavia and northern Germany: a review. In M.Wilson, E. R. Neumann, G. R. Davies, M.J. Timmerman, M. Heeremans & Larsen, B.T. (Eds). *Permo-Carboniferous Magmatism and Rifting in Europe (pp. 11-40)*. Geological Society, London, Special Publications, 223. DOI: 10.1144/GSL.SP.2004.223.01.02

Oftedahl, C., & Petersen, J.S.,1978. Southern part of the Oslo Rift. *Norges geologiske undersøkelse Bulletin, 337*, 163-182.

Petersen, J.S. (1978). Structure of the larvikite-lardalite complex, Oslo Region, Norway, and its evolution. *Geologisches Rundschau, 67*(1), 330-342.

Pfaff, K., Wenzel, T., Schilling, J., Marks, M.A.W, & Markl, G. (2010). A fast and easy-to-use approach to cation site assignment for eudialyte-group minerals. *Neues Jarhbuch fur Mineralogie, Abhandlungen, 187*(1), 69-81. DOI: 10.1127/0077-7757/2010/0166

Piilonen, P., Lalonde, A.E., McDonald, A.M., Gault, R.A., & Larsen, A.O. (2003). Insights into astrophyllite-group minerals. I. Nomenclature, Composition and development of a standardized general formula. *The Canadian Mineralogist, 41*, 1-26. DOI: 10.2113/gscanmin.41.1.1

Pouchou, J.L., & Pichoir, F. (1984). A new model for quantitative X-ray microanalysis. I. Application to the analysis of homogeneous samples. *La Recherche Aérospatiale, 3*, 13-38.

Raade, G., & Mladeck, M.H. (1977). Parakeldyshite from Norway. *The Canadian Mineralogist, 15*, 102-107.

Raade, G., & Mladeck, M.H., (1983). Janhaugite, $Na_3Mn_3Ti_2Si_4O_{15}(OH,F,O)_3$, a new mineral from Norway. *American Mineralogist, 68*, 1216-1219.

Sahama, T.G., (1978). The Nyiragongo main cone. *Musée Royale de l'Afrique Centrale. Annales Scieces Géologique Série in-8, 81*, 1–88.

Salvi, S., & Williams-Jones A.E. (1995). Zirconosilicate phase relations in the Strange Lake (Lac Brisson) pluton, Quebec-Labrador, Canada. *American Mineralogist, 80*, 1031-1040.

Sokolova, E. (2006). From structure topology chemical composition. I. Structural hierarchy and stereochemistry in titanium disilicate minerals. *The Canadian Mineralogist, 44*, 1273-1330. DOI: 10.2113/gscanmin.44.6.1273

Sokolova, E., & Cámara, F. (2008). From structure topology to chemical composition.VIII. Titanium silicates: the crystal chemistry of mosandrite from type locality of Låven (Skådön), Langesundsfjorden, Larvik, Vestfold, Norway. *Mineralogical Magazine, 72*(4), 887-897. DOI: 10.1180/minmag.2008.072.4.887

Strunz, H., & Nickel, E.H. (2001). *Strunz mineralogical tables*. 9th Edition. Stuttgart: E. Schweizerbart'sche Verlagsbuchhandlung (Nägle u. Obermiller).

Sæbø, P.C.1966. The first occurrence of the rare mineral barylite, $Be_2BaSi_2O_7$, in Norway. *Norsk Geologisk Tidsskrift, 46*, 335-348.

Sørensen, H., (1997). The agpaitic rocks – an overview. *Mineralogical Magazine, 61*(4), 485-498.

Ussing, N.V. (1912). Geology of the country around Julianehaab, Greenland. *Meddelelser om Grønland, 38*, 1-376

Weibye, P.H. (1850). Neue Mineralien aus Norwegen, beschrieben von P.H. Weibye; analysiert von N.J. Berlin, K.A. Sjögren und J.B. von Borck (Erster Theil). *Annalen der Physik und Chemie, 79*, 299-304.

Electron microprobe analyses of astrophyllite from LPC pegmatites

	A5-1	A5-2	A5-3	A5-4	A5-5	A5-6	A5-7	A5-8	A5-9	A5-10 Vein	A5-11 Vein	A5-12	A5-13	A5-14	A5-15	A4-16	A4-17	A4-18	A4-19	A4-20	A4-21	E2-35	E2-36	E2-37
Weight percent oxides																								
SiO_2	33.45	33.60	33.19	33.51	33.34	33.32	33.99	33.57	34.05	36.01	35.90	33.60	33.88	33.46	34.38	33.86	33.61	33.94	34.44	34.24	35.35	33.35	33.96	33.69
Al_2O_3	1.12	1.68	1.07	1.15	1.24	1.25	1.23	1.35	1.17	0.29	0.51	1.11	1.12	1.16	0.90	1.07	1.08	0.95	0.89	1.02	0.66	1.65	1.39	1.39
Nb_2O_5	0.66	1.64	0.54	0.66	3.00	0.82	1.59	0.95	0.60	0.15	0.32	1.05	0.69	3.15	0.87	1.51	1.41	1.32	1.53	1.44	0.22	2.41	2.16	2.80
ZrO_2	4.25	2.42	4.02	4.25	0.80	3.68	1.02	3.58	4.09	0.08	0.11	3.80	3.98	0.88	0.91	3.72	3.67	3.37	3.36	3.25	1.39	4.20	4.27	4.52
HfO_2	0.12	0.11	0.11	0.14	0.08	0.13	0.10	0.11	0.09	0.02	0.05	0.18	0.27	0.10	0.06	0.06	0.19	0.03	0.16	0.12	0.02	0.24	0.34	0.26
TiO_2	8.74	9.42	8.67	8.48	7.57	8.78	10.20	8.96	8.87	11.19	11.10	8.87	9.03	7.50	11.09	8.47	8.60	9.03	8.96	9.04	11.03	7.72	7.65	7.53
La_2O_3	0.21		0.22	0.22	0.03	0.15		0.13	0.07		0.02	0.18	0.13	0.08	0.12	0.06	0.07	0.01	0.05	0.08		0.01		
Ce_2O_3	0.13	0.03	0.25	0.27		0.25		0.42	0.20		0.01	0.34	0.23		0.15	0.12	0.10	0.04	0.35	0.20				
Nd_2O_3	0.23		0.16	0.04	0.02	0.01			0.01	0.11		0.00	0.11	0.08	0.03	0.01	0.08	0.09	0.01	0.06				0.06
FeO	22.72	24.14	23.29	23.11	24.18	23.79	25.58	24.50	24.18	28.27	28.26	22.59	23.42	24.08	23.98	17.89	18.21	19.76	19.10	17.91	19.84	20.17	20.25	20.11
MgO	0.94	0.60	0.60	0.81	0.69	0.70	0.53	0.52	0.55	0.16	0.27	0.88	0.64	0.61	0.73	1.00	0.92	0.82	0.86	1.04	0.96	0.83	0.75	0.85
MnO	11.12	10.83	11.17	11.37	10.22	11.50	9.85	10.90	11.75	9.02	8.45	11.56	11.46	11.20	11.41	16.86	16.47	15.35	15.48	16.35	16.02	15.45	15.37	15.61
CaO	0.91	1.21	0.88	0.91	0.68	0.91	0.89	0.90	0.93	0.26	0.36	1.01	0.76	0.72	1.08	0.93	0.71	0.71	0.83	0.97	0.83	1.37	1.14	1.22
Na_2O	2.21	2.04	2.25	2.19	2.32	2.22	2.32	2.15	2.25	5.31	4.92	2.37	2.40	2.39	2.42	2.40	2.38	2.40	2.43	2.23	2.70	1.93	1.96	1.99
K_2O	5.43	5.88	5.44	5.47	5.64	5.62	5.68	5.67	5.62	1.14	1.42	5.42	5.42	5.49	5.39	5.76	5.68	5.60	5.71	5.83	5.64	6.10	6.24	6.14
F	1.30	0.86	0.98	1.23	1.11	1.04	1.05	1.54	1.73	1.52	1.26	0.99	1.05	0.95	1.17	1.32	0.91	1.33	1.19	1.40	1.55	1.35	1.51	1.16
$O=F$	-0.55	-0.36	-0.41	-0.52	-0.47	-0.44	-0.44	-0.65	-0.73	-0.64	-0.53	-0.42	-0.44	-0.40	-0.49	-0.56	-0.38	-0.56	-0.50	-0.59	-0.65	-0.57	-0.63	-0.49
Sum	93.02	94.11	92.42	93.29	90.42	93.71	93.60	94.59	95.43	92.88	92.42	93.52	94.15	91.43	94.18	94.47	93.69	94.19	94.83	94.59	95.54	96.19	96.35	96.84

Structural formulas based on 20,000 cations

Si	7.781	7.67	7.76	7.77	7.88	7.67	7.76	7.70	7.74	8.14	8.16	7.75	7.78	7.84	7.79	7.71	7.72	7.76	7.83	7.80	7.85	7.54	7.67	7.58
Al	0.308	0.45	0.29	0.31	0.35	0.34	0.33	0.36	0.31	0.08	0.14	0.30	0.30	0.32	0.24	0.29	0.29	0.26	0.24	0.27	0.17	0.44	0.37	0.37
Nb	0.070	0.17	0.06	0.07	0.32	0.09	0.16	0.10	0.06	0.01	0.03	0.11	0.07	0.33	0.09	0.16	0.15	0.14	0.16	0.15	0.02	0.25	0.22	0.29
Zr	0.482	0.27	0.46	0.48	0.09	0.41	0.11	0.40	0.45	0.01	0.01	0.43	0.45	0.10	0.10	0.41	0.41	0.38	0.37	0.36	0.15	0.46	0.47	0.50
Hf	0.008	0.01	0.01	0.01	0.01	0.01	0.01	0.01	0.01	0.00	0.00	0.01	0.02	0.01	0.00	0.00	0.01	0.00	0.01	0.01	0.00	0.02	0.02	0.02
Ti	1.530	1.62	1.53	1.48	1.35	1.52	1.75	1.55	1.52	1.90	1.90	1.54	1.56	1.32	1.89	1.45	1.49	1.55	1.53	1.55	1.84	1.31	1.30	1.28
La	0.018		0.02	0.02	0.00	0.01		0.01	0.01		0.00	0.02	0.01	0.01	0.01	0.00	0.01	0.00	0.00	0.01		0.00		
Ce	0.011		0.02	0.02	0.00	0.02		0.03	0.02		0.00	0.03	0.02		0.01	0.01	0.01	0.00	0.03	0.02				
Nd	0.019	0.00	0.01	0.00	0.00	0.00			0.00	0.01		0.00	0.01	0.01	0.00	0.00	0.01	0.01	0.00	0.00				0.00
Fe	4.420	4.61	4.56	4.48	4.78	4.58	4.89	4.70	4.59	5.35	5.37	4.36	4.50	4.72	4.54	3.41	3.50	3.78	3.63	3.41	3.68	3.81	3.83	3.78
Mg	0.325	0.20	0.21	0.28	0.24	0.24	0.18	0.18	0.19	0.05	0.09	0.30	0.22	0.21	0.25	0.34	0.31	0.28	0.29	0.35	0.32	0.28	0.25	0.28
Mn	2.191	2.09	2.21	2.24	2.05	2.24	1.91	2.12	2.26	1.73	1.63	2.26	2.23	2.22	2.19	3.25	3.20	2.97	2.98	3.15	3.01	2.96	2.94	2.98
Ca	0.228	0.30	0.22	0.22	0.17	0.22	0.22	0.22	0.23	0.06	0.09	0.25	0.19	0.18	0.26	0.23	0.17	0.17	0.20	0.24	0.20	0.33	0.27	0.29
Na	0.998	0.90	1.02	0.98	1.06	0.99	1.03	0.96	0.99	2.33	2.17	1.06	1.07	1.08	1.06	1.06	1.06	1.06	1.07	0.99	1.16	0.84	0.86	0.87
K	1.612	1.71	1.62	1.62	1.70	1.65	1.66	1.66	1.63	0.33	0.41	1.60	1.59	1.64	1.56	1.67	1.66	1.63	1.66	1.69	1.60	1.76	1.80	1.76
F	0.958	0.62	0.73	0.91	0.83	0.76	0.76	1.12	1.25	1.09	0.91	0.72	0.77	0.70	0.84	0.95	0.66	0.96	0.86	1.01	1.09	0.96	1.08	0.82

Electron microprobe analyses of rinkite- and rosenbuschite group minerals from LPC pegmatites

	LV01 #M01 Mos	LV01 #M02 Mos	LV01 #M03 Mos	LV01 #M04 Mos	LV01 #01 Koc (?)	LV01 #02 Koc (?)	LV01 #04 Hio	LV01 #11 Hio	LV01 #1 Mos	LV01 #2 Mos	LV01 #5 Mos	LV01 #6 Mos	LV01 #7 Mos	LV01 #8 Mos	LV08 #M05 Mos	LV08 #M06 Mos	LV08 #M07 Mos	LV08 #M08 Mos	LV08 #M09 Mos	LV08 #M10 Mos	LV13 #M102 Mos	LV13 #M103 Mos	LV13 #M104 Mos
Weight percent oxides																							
SiO_2	29.27	28.61	28.37	28.62	30.82	30.82	30.27	29.99	30.03	29.98	13.42	29.21	28.85	28.82	29.01	29.32	29.13	28.58	27.80	27.60	26.67	26.38	26.30
ZrO_2	1.84	1.77	1.61	1.71	11.31	10.90	16.90	16.51	1.23	1.41	1.50	1.00	1.15	1.14	1.67	1.76	1.44	1.54	1.79	1.42	1.67	1.93	1.75
HfO_2			0.04	0.07	0.27	0.01	0.43	0.49		0.10	0.02	0.02	0.02	0.04	0.03	0.04	0.01	0.10	0.11	0.04	0.03	0.06	0.02
Nb_2O_5	1.87	1.93	1.80	1.71	1.07	1.02	2.10	1.87	1.56	1.52	0.00	1.28	1.39	1.50	1.53	1.85	1.65	2.22	2.00	1.71	1.38	1.54	1.53
ThO_2	1.14	1.27	1.09	1.19	0.06	0.00	0.00	0.00	0.93	0.79	0.89	0.95	0.97	0.85	0.77	1.03	1.10	1.41	1.33	1.29	1.08	1.30	1.17
TiO_2	9.86	9.98	10.27	9.87	9.90	10.45	0.93	0.89	9.43	9.15	0.50	9.72	9.46	9.44	9.79	9.83	9.79	10.03	10.47	10.11	9.13	9.32	9.50
Y_2O_3	0.12	2.47	2.45	2.53	2.19	2.46	1.00	0.47	0.24	0.07	0.31	0.10	0.14	4.09	2.91	3.04	2.91	3.67	3.76	3.58	2.96	2.86	2.88
La_2O_3	4.76	4.80	5.09	4.65	0.18	0.10	0.17	0.06	3.95	3.93	9.40	4.98	4.60	4.58	3.75	3.77	4.20	5.00	5.41	5.15	5.08	5.22	5.06
Ce_2O_3	9.25	9.04	9.50	9.06	0.32	0.30	0.45	0.13	8.33	8.69	21.81	9.37	9.78	8.82	8.22	8.28	8.85	10.75	11.60	10.99	10.45	10.52	9.56
Nd_2O_3	2.57	2.88	2.66	2.47	0.12	0.25	0.16	0.12	2.94	3.01	6.27	3.22	3.07	3.36	2.41	2.77	2.76	3.50	3.94	3.64	2.81	2.56	2.66
Al_2O_3	0.45	0.44	0.51	0.50					0.35	0.24		0.62	0.49	0.42	1.03	0.97	1.14	1.04	1.91	1.11	0.69	0.78	0.90
CaO	16.98	16.92	16.44	17.12	22.04	22.71	31.48	33.05	17.13	18.70	11.20	14.88	15.80	16.62	18.03	17.55	16.77	12.93	10.08	12.26	14.39	14.39	14.10
FeO	0.24	0.26	0.23	0.23	0.37	0.28	1.24	1.23	0.03	0.02	0.88	0.07	0.01	0.04	0.18	0.10	0.11	0.06	0.07	0.03	3.82	4.36	4.10
MnO	0.55	0.66	0.78	0.79	4.31	3.40	1.32	0.92	0.29	0.23	0.19	0.58	0.37	0.28	0.29	0.45	0.38	0.34	0.28	0.33	0.12	0.20	0.24
Na_2O	0.71	0.66	0.60	0.78	10.02	9.96	7.15	6.71	1.55	2.11	1.14	1.21	1.24	1.41	1.75	1.43	1.43	0.88	0.68	0.92	0.59	0.50	0.50
K_2O	0.08	0.08	0.08	0.06	0.02	0.00	0.02	0.01	0.04	0.09	0.01	0.28	0.13	0.11	0.17	0.16	0.16	0.15	0.18	0.16	0.08	0.10	0.10
F	2.15	8.26	2.87	1.41	7.59	7.82	7.86	9.01	3.57	2.60	8.71	0.00	1.25	2.56	1.94	2.41	1.47	1.52	1.38	1.61		0.46	0.58
O=F	-0.90	-3.48	-1.21	-0.60	-3.19	-3.29	-3.31	-3.80	-1.50	-1.10	-3.67	0.00	-0.53	-1.08	-0.82	-1.02	-0.62	-0.64	-0.58	-0.68	0.00	-0.19	-0.25
Total	80.93	86.54	83.18	82.17	97.37	97.21	98.16	97.68	80.10	81.53	72.60	77.49	78.21	83.02	82.66	83.76	82.69	83.08	82.23	81.26	80.96	82.26	80.69

Structural formulas based on 4.00 Si

Si	4.00	4.00	4.00	4.00	4.00	4.00	4.00	4.00	4.00	4.00	4.00	4.00	4.00	4.00	4.00	4.00	4.00	4.00	4.00	4.00	4.00	4.00	4.00	4.00
Zr+Hf	0.12	0.12	0.11	0.12	0.69	1.11	1.09	0.08	0.10	0.22	0.07	0.08	0.08	0.11	0.12	0.11	0.10	0.11	0.13	0.10	0.13	0.12	0.14	0.13
Ti	1.01	1.05	1.09	1.04	1.02	0.09	0.09	0.95	0.92	0.11	1.00	0.99	0.99	1.02	1.01	1.06	1.01	1.06	1.13	1.10	1.13	1.03	1.06	1.09
Nb	0.12	0.12	0.11	0.11	0.06	0.13	0.11	0.09	0.09	0.00	0.08	0.09	0.10	0.10	0.11	0.14	0.10	0.13	0.13	0.11	0.13	0.09	0.11	0.11
Th	0.04	0.04	0.03	0.04	0.06	0.13	0.11	0.03	0.02	0.06	0.03	0.03	0.02	0.02	0.03	0.04	0.03	0.04	0.04	0.04	0.04	0.04	0.04	0.04
REE[1]	0.84	1.04	1.07	1.01	0.20	0.11	0.05	0.76	0.77	4.13	0.89	0.89	0.94	0.94	0.96	1.26	1.01	1.15	1.39	1.32	1.24	1.24	1.24	1.19
Al	0.07	0.07	0.08	0.08		0.14		0.06	0.04		0.10	0.07	0.17	0.16	0.16	0.17	0.18	0.32	0.32	0.19	0.12	0.14	0.12	0.16
Fe	0.03	0.03	0.03	0.03	0.03	0.14	0.14	0.00	0.00	0.22	0.01	0.00	0.02	0.02	0.01	0.01	0.01	0.01	0.00	0.00	0.48	0.55	0.52	
Mn	0.06	0.08	0.09	0.09	0.37	0.15	0.10	0.03	0.03	0.05	0.07	0.04	0.03	0.03	0.05	0.04	0.04	0.03	0.04	0.03	0.02	0.03	0.03	0.03
Ca	2.49	2.53	2.48	2.56	3.16	4.46	4.72	2.45	2.67	3.58	2.18	2.35	2.47	2.66	2.57	1.94	2.47	1.94	1.55	1.90	2.31	2.34	2.30	
Na	0.19	0.18	0.16	0.21	2.51	1.83	1.74	0.40	0.54	0.66	0.32	0.33	0.38	0.47	0.38	0.24	0.38	0.24	0.19	0.26	0.17	0.15	0.15	
K	0.01	0.01	0.01	0.00	0.00	0.00	0.00	0.01	0.02	0.00	0.05	0.02	0.02	0.03	0.03	0.03	0.03	0.03	0.03	0.02	0.02	0.02		
F	0.93	3.65	1.28	0.63	3.21	3.28	3.80	1.50	1.10	8.21	0.00	0.55	1.12	0.85	1.04	0.67	0.64	0.63	0.74	0.63	0.22	0.28		
SumCat	8.97	9.28	9.29	9.30	12.04	12.01	12.04	8.85	9.20	13.03	8.79	8.91	9.31	9.57	9.42	9.03	9.37	9.03	9.11	8.97	9.64	9.82	9.73	
Vac	3.03	2.72	2.71	2.70	-0.04	-0.01	-0.04	3.15	2.80	-1.03	3.21	3.09	2.69	2.43	2.58	2.97	2.63	3.03	2.89	2.36	2.18	2.27		

Abbreviations: Mos= Mosandrite, Ros= Rosenbuschite, Koc= Kochite, Hai= Hainite, Hio= Hiortdahlite,

1: REE = La+Ce+Nd+Y

	LV03 #116 Mos	LV03 #112 Hai	LV03 #113 Hai	LV03 #114 Hai	LV03 #115 Hai	LV03 #117 Hai	LV03 #119 Hai	LV09 #20 Ros	LV09 #21 Ros	LV09 #22 Ros	LV09 #23 Ros	LV09 #24 Ros	LV09 #26 Ros	LV09 #27 Ros	SAG1 #48 Ros	SAG1 #49 Ros	SAG1 #50 Hai	SAG1 #51 Hai	SAG1 #52 Hai
Weight percent oxides																			
SiO$_2$	25.48	30.47	29.69	29.79	30.04	29.75	29.87	30.62	30.01	30.75	30.25	30.55	30.28	30.56	31.37	31.54	30.92	30.90	30.37
ZrO$_2$	0.08	4.78	4.26	5.02	3.32	4.84	4.57	12.54	11.77	12.91	9.95	13.49	16.30	16.56	16.02	15.34	7.11	6.89	5.84
HfO$_2$	0.00	0.08	0.12	0.15	0.07	0.15	0.11	0.30	0.29	0.32	0.22	0.32	0.40	0.33	0.23	0.23	0.17	0.14	0.11
Nb$_2$O$_5$	0.35	1.29	1.07	1.53	1.18	1.52	1.63	0.65	1.25	0.83	1.07	0.83	1.04	1.05	0.08	0.08	0.91	0.99	0.79
ThO$_2$	0.39	0.15	0.18	0.24	0.18	0.20	0.12	0.01	0.01	0.06	0.05	0.06	0.08	0.00	0.01	0.03	0.10	0.11	0.14
TiO$_2$	5.17	8.12	8.25	8.14	8.26	8.00	8.10	8.36	6.85	8.46	7.46	8.20	5.90	7.03	7.90	8.32	8.09	8.16	8.37
Y$_2$O$_3$	0.18	0.27	3.75	3.45	3.84	3.63	0.36	3.04	3.90	0.08	3.39	0.19	1.54	1.14	0.03	0.09	2.02	2.00	2.21
La$_2$O$_3$	2.92	0.91	1.03	0.90	1.52	0.84	0.97	0.07	0.09	0.04	0.44	0.09	0.12	0.08	0.00	0.02	0.73	0.72	0.96
Ce$_2$O$_3$	8.58	2.12	2.17	2.12	3.33	2.03	1.84	0.17	0.43	0.17	1.21	0.25	0.39	0.10	0.08	0.10	1.59	1.76	2.15
Nd$_2$O$_3$	3.35	0.69	1.02	0.62	1.12	0.67	0.86	0.16	0.19	0.03	0.38	0.04	0.17	0.05	0.00	0.12	0.79	0.76	0.90
Al$_2$O$_3$	0.73														0.05	0.07	0.04	0.02	
CaO	22.22	31.12	30.96	30.90	30.13	30.55	30.82	24.48	25.28	24.64	26.47	24.73	23.75	23.48	28.06	28.05	31.97	31.93	32.09
FeO	0.97	0.52	0.42	0.36	0.26	0.40	0.49	0.19	0.23	0.20	0.28	0.21	0.44	0.37	0.47	0.74	0.43	0.46	0.35
MnO	0.83	0.83	0.73	0.67	0.54	0.73	0.66	1.94	1.66	1.97	1.74	1.99	1.87	2.10	0.96	0.86	0.57	0.63	0.47
Na$_2$O	0.24	7.56	7.54	7.50	7.76	7.45	7.57	9.60	8.92	9.40	8.62	9.48	9.60	9.86	9.14	9.01	7.65	7.45	7.49
K$_2$O				0.01	0.01		0.02	0.01	0.01		0.01		0.01		0.01	0.01	0.01	0.02	0.01
F	0.11	7.90	7.37	7.61	7.66	8.07	7.72	7.81	7.45	7.99	8.05	7.31	8.24	7.95	7.74	8.11	9.75	8.75	9.41
O=F	-0.05	-3.33	-3.10	-3.21	-3.22	-3.40	-3.25	-3.29	-3.14	-3.36	-3.39	-3.08	-3.47	-3.35	-3.26	-3.41	-4.11	-3.68	-3.96
Total	71.55	93.49	95.47	95.80	95.99	95.45	92.46	96.66	95.21	94.47	96.21	94.67	96.68	97.31	98.88	99.31	98.74	98.01	97.68

Structural formulas based on 4.00 Si

Si	4.00	4.00	4.00	4.00	4.00	4.00	4.00	4.00	4.00	4.00	4.00	4.00	4.00	4.00	4.00	4.00	4.00	4.00	4.00
Zr+Hf	0.01	0.31	0.28	0.33	0.22	0.32	0.30	0.81	0.78	0.83	0.65	0.87	1.07	1.07	1.00	0.96	0.45	0.44	0.38
Ti	0.61	0.80	0.84	0.82	0.83	0.81	0.82	0.82	0.69	0.83	0.74	0.81	0.59	0.69	0.76	0.79	0.79	0.79	0.83
Nb	0.02	0.08	0.07	0.09	0.07	0.09	0.10	0.04	0.08	0.05	0.06	0.05	0.06	0.06	0.00	0.00	0.05	0.06	0.05
Th	0.01	0.00	0.01	0.01	0.01	0.01	0.00	0.00	0.00	0.00	0.00	0.00	0.00	0.00	0.00	0.00	0.00	0.00	0.00
REE[1]	0.87	0.20	0.48	0.43	0.56	0.43	0.21	0.23	0.31	0.02	0.34	0.03	0.14	0.09	0.01	0.02	0.29	0.29	0.35
Al	0.13														0.01	0.01	0.01		
Fe	0.13	0.06	0.05	0.04	0.03	0.05	0.05	0.02	0.03	0.02	0.03	0.02	0.05	0.04	0.05	0.08	0.05	0.05	0.04
Mn	0.11	0.09	0.08	0.08	0.06	0.08	0.07	0.21	0.19	0.22	0.19	0.22	0.21	0.23	0.10	0.09	0.06	0.07	0.05
Ca	3.74	4.38	4.47	4.44	4.30	4.40	4.42	3.43	3.61	3.43	3.75	3.47	3.36	3.29	3.83	3.81	4.43	4.43	4.53
Na	0.07	1.92	1.97	1.95	2.00	1.94	1.97	2.43	2.31	2.37	2.21	2.41	2.46	2.50	2.26	2.22	1.92	1.87	1.91
K				0.00	0.00		0.00	0.00	0.00		0.00		0.00		0.00	0.00	0.00	0.00	0.00
F	0.06	3.28	3.14	3.23	3.22	3.43	3.27	3.22	3.14	3.29	3.37	3.03	3.44	3.29	3.12	3.25	3.99	3.58	3.92
SumCat	9.70	11.84	12.24	12.20	12.08	12.14	11.95	12.00	11.98	11.77	11.98	11.88	11.94	11.98	12.03	11.98	12.05	12.01	12.14
Vac	2.30	0.16	-0.24	-0.20	-0.08	-0.14	0.05	0.00	0.02	0.23	0.02	0.12	0.06	0.02	-0.03	0.02	-0.05	-0.01	-0.14